Palaeogeography, Palaeoclimatology, Palaeoecology 622 (2023) 111601

Contents lists available at ScienceDirect

Palaeogeography, Palaeoclimatology, Palaeoecology

journal homepage: www.elsevier.com/locate/palaeo

Role of climate variability on deep-water dynamics and deoxygenation during sapropel deposition: New insights from a palaeoceanographic empirical approach

Ricardo D. Monedero-Contreras [a,*], Francisca Martínez-Ruiz [a], Francisco J. Rodríguez-Tovar [b]

[a] Instituto Andaluz de Ciencias de la Tierra (CSIC-UGR), Armilla, Spain
[b] Departmento de Estratigrafía y Paleontología, Universidad de Granada, Granada, Spain

ARTICLE INFO

Editor: Prof. M. Elliot

Keywords:
Mediterranean
Sapropel
Deoxygenation
Climate change
Trace metal
Palaeoceanography

ABSTRACT

Modern marine settings are experiencing rapid deoxygenation mainly forced by global warming and anthropogenic eutrophication. Therefore, studies that assess the role of climate variability in large spatiotemporal deoxygenations during past climate changes are needed to better comprehend the consequences of the current global warming and ocean deoxygenation. In this respect, deep marine sediments associated to past oxic-to-anoxic transitions are useful palaeoarchives for understanding the interplay between climate variability, deep-water dynamics and large-scale deoxygenation. Moreover, they can offer long-term perspectives to modern marine settings that are suffering oxygen depletion due to climate change and anthropogenic pressure. In particular, sapropel layers from the Middle Pleistocene to the Holocene are excellent palaeoarchives of past large-scale deoxygenation events, since (i) they occurred during a similar Mediterranean hydrogeographic configuration to the present, (ii) have a robust chronological control, and (iii) previous studies have reconstructed the climate conditions that ruled during their deposition. In this work, we have applied empirical palaeoceanographic conceptual models to five sapropels (S1, S5, S6, S7 and S8) in three Eastern Mediterranean (EM) settings. The models suggest that the hydrographic regimes of all studied sapropels can be considered as analogues to those observed in certain modern marine restricted settings. The results obtained support the idea that climate and the degree of surface-water freshening are the primary factors that influence deep-water dynamics in marine restricted settings, that in turn control the frequency and intensity of bottom-water deoxygenation and the stability and depth of the chemocline. The deepest EM sites are the most vulnerable locations to develop bottom-water restriction and deoxygenation. Local hydrogeographic factors play an essential role in the extent and frequency of bottom-water deoxygenation. Particulate shuttling was very intense during sapropel deposition and water-mass exchange between EM and Western Mediterranean controlled the intensity of the basin reservoir effect and Mo budget in EM.

1. Introduction

An oxygen loss between 1 and 7% in oxygen is expected by 2100 in most marine areas around the globe (Breitburg et al., 2018). Deoxygenation is considered one of the most impacting ocean stressors in present marine systems, since a decrease in oxygen content alters productivity, biodiversity and biogeochemical cycles (Levin, 2018). Although deoxygenation can be linked to increased productivity, deep-water dynamics also play a major role in the intensity, duration and extent of deoxygenation (van Santvoort and de Lange, 1996; Warning and Brumsack, 2000; Gallego-Torres et al., 2007a; Algeo and Tribovillard, 2009; Gallego-Torres et al., 2012; Grimm et al., 2015; Levin, 2018; Algeo and Li, 2020; Lathika et al., 2021). Nonetheless, little is known about the interplay of climate conditions with large-scale deoxygenation and deep-water circulation, and about the influence of local hydrogeographic factors.

Palaeoceanographic reconstructions of past large-scale deoxygenations linked to climate variability are crucial to better understand the responses of modern marine systems vulnerable to experience oxygen loss due to the current climate change and anthropogenic pressure (Stocker et al., 2013; Levin, 2018; Dermawan et al., 2022). In this regard, sapropels, as layers with TOC (total organic carbon) content

* Corresponding author.
E-mail address: ricardo.monedero@csic.es (R.D. Monedero-Contreras).

https://doi.org/10.1016/j.palaeo.2023.111601
Received 5 September 2022; Received in revised form 26 April 2023; Accepted 26 April 2023
Available online 27 April 2023

above 2%, represent rapid oxic-to-anoxic transitions induced by rapid climate variability (over time scales of hundreds of years or even decades) (Cita et al., 1977). Therefore, they can offer relevant insights about the role of climate change on large-scale deoxygenation and deep-water dynamics (Marino et al., 2007; Grimm et al., 2015; Benkovitz et al., 2020; Blanchet et al., 2020; Hennekam et al., 2020). Moreover, large-scale deoxygenations during sapropels deposition over the Pleistocene-Holocene occurred during a similar hydrogeographic configuration as today, thus allowing to make palaeooceanographic inferences from modern oceanographic observations (Rohling et al., 2015).

In the Eastern Mediterranean (EM), the deposition of sapropels is controlled by astronomical precession cycles (Kidd et al., 1978; Calvert, 1983; Emeis et al., 1996, 2000). Minimum astronomical precession periods caused periods of maximum insolation in the northern hemisphere, which produced an intensification and a northward migration of the African monsoons, resulting in greater discharge of fresh-water and nutrients into the EM (De Lange et al., 1989; Hilgen, 1991; Lourens et al., 1996; Hennekam et al., 2014; Weldeab et al., 2014; Rohling et al., 2015; Tachikawa et al., 2015). The increased marine productivity and weakened water-column circulation (reduced vertical mixing), resulting in oxygen depletion in the bottom-waters, promoted the deposition and preservation of organic-rich sapropels (Cita and Grignani, 1982; Rossignol-Strick, 1985; Rohling, 1994; Gallego-Torres et al., 2007a, 2007b, 2010; Marino et al., 2009; Rohling et al., 2015; Zwiep et al., 2018).

In this context, this work assesses the consequences of past climate variability on water-column dynamics and redox conditions in bottom-waters during sapropel deposition. This is achieved by applying different palaeoceanographic conceptual models based on empirical geochemical data (trace metal concentration and TOC%) obtained from well-studied modern marine systems (Algeo and Lyons, 2006; Algeo et al., 2007; Algeo and Maynard, 2008; McArthur et al., 2008; Algeo and Tribovillard, 2009; Tribovillard et al., 2012; Sweere et al., 2016; McArthur, 2019). These conceptual palaeoceanographic models have been applied to five recent sapropels (S1, S5, S6, S7 and S8) from three EM locations that represent different oceanographic regimes (Figs. 1 and

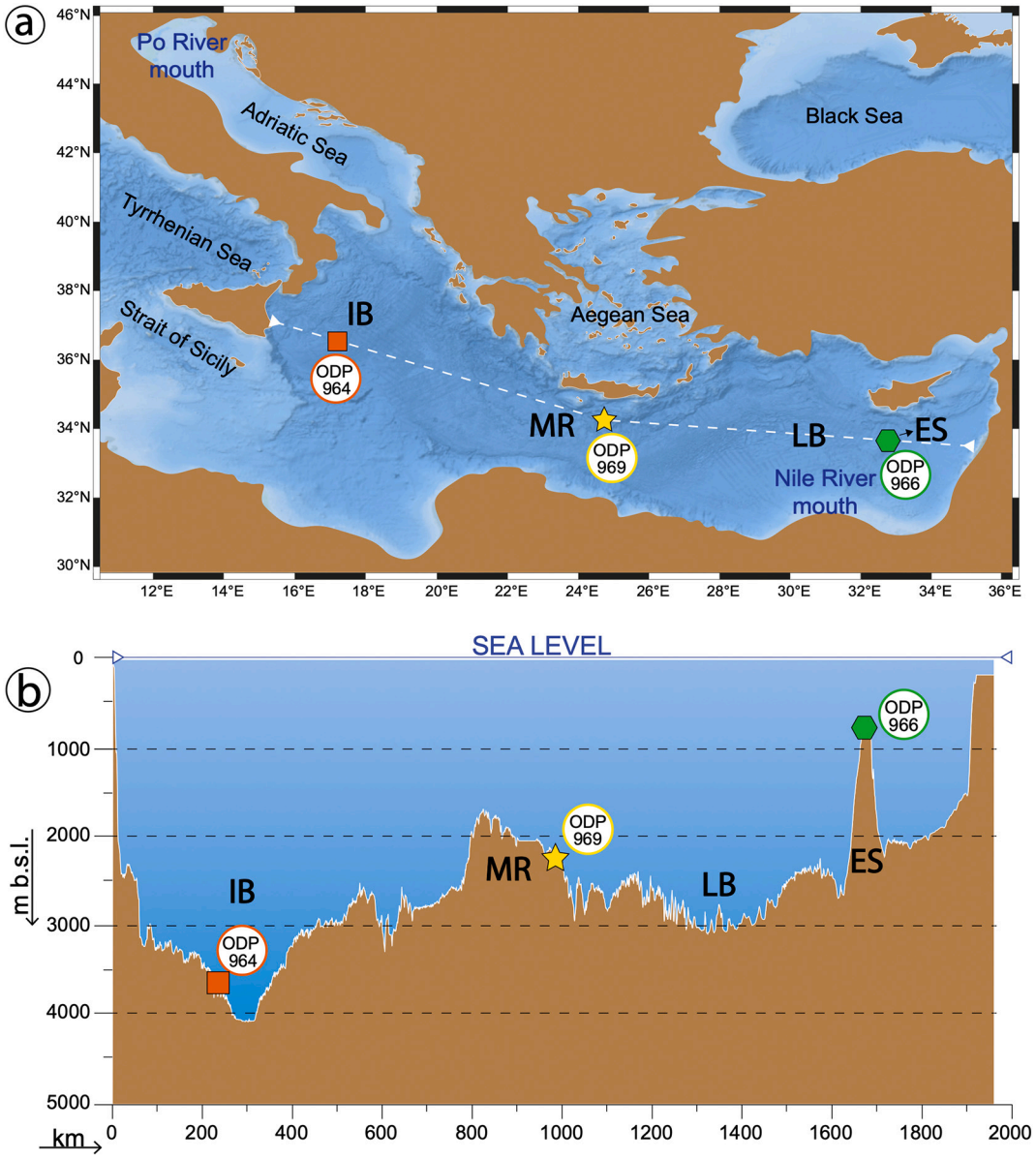

Fig. 1. (a) Satellite image showing the location of the three studied ODP sites (964, 966 and 969); (b) bathymetric section showing the depth of the three ODP sites; available under the European Marine Observation Data Network (EMODnet) Seabed Habitats initiative (http://www.emodnet-seabedhabitats.eu/). ES: Eratosthenes Seamount, IB: Ionian Basin, LB: Levantine Basin, MR: Mediterranean Ridge.

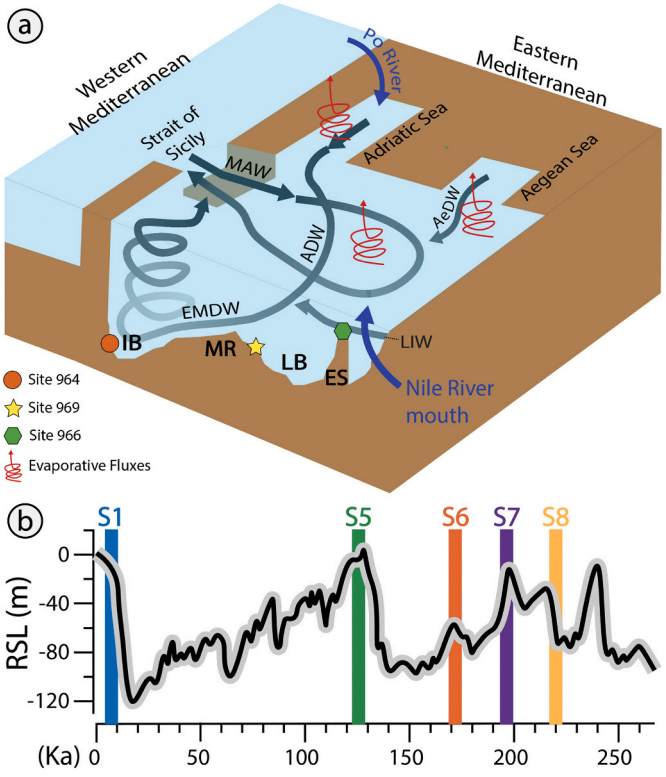

Fig. 2. (a) 3D scheme (not to scale) of the modern EM circulation modified from Lascaratos et al. (1999), showing the main EM water-masses, currents and deep-water formation sites, and the main fresh-water inputs (fluvial inputs). IB: Ionian Basin (site 964), MR: Mediterranean Ridge (site 969), ES: Eratosthenes Seamount (site 966), LB: Levantine Basin. Water-masses: ADW (Adriatic Deep Water), AeDW (Aegean Deep Water), EMDW (Eastern Mediterranean Deep Water), LIW (Levantine Intermediate Water), and MAW (Modified Atlantic Water). (b) Approximate relative sea-level (RSL) for the last 250 ka from Grant et al. (2014). Time interval of each sapropel is indicated (Ziegler et al., 2010; Grant et al., 2016).

2). The models provided key insights into (i) the consequences of past climate variability on water-column dynamics and physicochemical properties, (ii) the influence of local hydrogeographic features (i.e., water-depth, proximity to continental borderlands, local active currents) on bottom-water dynamics and redox conditions, (iii) the extent of deep-water restriction and intensity of deoxygenation in EM during rapid climate changes, and (vi) long-term perspectives about modern marine settings vulnerable to develop oxygen deficiency in the near future.

2. Oceanographic and palaeoceanographic setting

The Mediterranean Sea is a complex marine system with a strong thermohaline circulation that allows deep-water masses to renew and oxygenate (Pinardi and Masetti, 2000; Millot and Taupier-Letage, 2005; Pinardi et al., 2015; Rohling et al., 2015). In general, it represents an exceptional natural laboratory to study the impacts of past and current climate changes since: (i) it is one of the most vulnerable regions or hotspots to climate change on Earth, (ii) it is very responsive to external and climate forcing (e.g., orbital forcing, anthropogenic forcing), (iii) it amplifies and anticipates marine responses to global climate change (its turnover timescale is about one tenth of the global ocean's), and (iv) its sedimentary record has remarkably preserved marine responses to past climate changes (Calvert, 1983; Emeis et al., 1996, 2000; Giorgi, 2006; Lionello et al., 2006; Rohling et al., 2015; Turco et al., 2015; Schroeder et al., 2016). These features derive from its geographic and oceanographic setting; latitude (transitional zone), semi-enclosed (restricted) marginal sea, relatively small area (~2,500,000 km^2), deep water-depth (over 5000 m), hydrological balance (high evaporation rate), complex land-sea distribution and seafloor morphology.

Today, the main three mechanisms controlling Mediterranean Sea circulation are wind stress, thermohaline forcing and Atlantic water-exchange (POEM Group, 1992; Millot and Taupier-Letage, 2005; Amitai et al., 2018). Atlantic Water (AW) enters the Mediterranean Sea through the Strait of Gibraltar and mixes with upwelled and saltier Mediterranean Intermediate Water (MIW), resulting in the formation of Modified Atlantic Water (MAW; upper 200 m to down to 600-1000 m water-depth) (Millot, 1999, 2009). Then MAW splits into a northward current and an eastward current. The eastward current passes through the Strait of Sicily (EM gateway; water-depth ~ 350 m) and reaches the EM (Fig. 2; Millot, 1999, 2009; Millot and Taupier-Letage, 2005). During winter-cooling, strong northern winds with dry and cold air masses evaporate Levantine Basin surface-water, increasing its salinity (i.e., density) and stimulating vertical convection, resulting in the formation of the Levantine Intermediate Water (LIW; between ~150 and ~ 600 m water-depth) (Lascaratos et al., 1999; Millot, 1999, 2009; Millot and Taupier-Letage, 2005; Pinardi et al., 2015; Rohling et al., 2015 and references therein).

LIW contributes to the formation of the Easter Mediterranean Deep Water (EMDW). However, EMDW is mainly formed in the Adriatic Sea region and to a lesser extent, in the Aegean Sea region (Fig. 2; Wüst, 1961; Miller, 1963; Lascaratos et al., 1999; Millot and Taupier-Letage, 2005). In winter, Adriatic shelf water becomes cooler and its salinity increases under the action of cold and dry north-easterly winds (Ozsoy, 1981; Astraldi and Gasparini, 1992; Sparnocchia et al., 1994). Shelf waters sink towards the deep south of the Adriatic Basin, where it mixes with LIW and leads to the formation of the Adriatic Deep Water (ADW). ADW reaches the abyssal Ionian Basin, where it becomes the major contributor for EMDW circulation (Fig. 2; POEM Group, 1992; Amitai et al., 2018).

In recent decades, temperature, salinity and density of Mediterranean deep-water masses have increased, while deep-water convection and oxygen content have significantly decreased (Roether et al., 1996; Sparnocchia et al., 2006). In fact, from 1950 to 2010, the Mediterranean below 1000 m underwent the strongest salinity gain anywhere in the world and have suffered important oceanographic changes that weakened deep-water circulation (e.g., *Western Mediterranean Transition* and *Eastern Mediterranean Transient*) (Lascaratos et al., 1999; Malanotte-Rizzoli et al., 1999; Skliris et al., 2014; Schroeder et al., 2016). These oceanographic changes have been partially attributed to anthropogenic disturbances, such as the damming of the Nile in 1964, which has increased by ~30% the formation rate of LIW, which explains ~45% of the salinity increase in Western Mediterranean Deep Water and contributed to triggered *Eastern Mediterranean Transient* (Skliris and Lascaratos, 2004).

In general, the present EM thermohaline circulation and low primary productivity promote oxic and ultra-oligotrophic conditions in the water-column, low TOC content in sediments (from 0.1 to 0.2%) and a conservative behavior of Mo and U as in global ocean ([U] ~3.23 ng/g, ([Mo] ~10 ng/g) (Abbott, 1977; Morford and Emerson, 1999; Delanghe et al., 2002; Rohling et al., 2015). However, during sapropel deposition weakened anti-estuarine circulation and increased fresh-water discharge, reduced vertical-mixing and decreased surface-water salinity (Rohling et al., 2015; Zirks et al., 2019). The main fresh-water inputs came from the Nile River and palaeo African drainages (Gallego-Torres et al., 2007a; Rohling et al., 2015; Tachikawa et al., 2015; Wu et al., 2016, 2018), although during some cold sapropel events (e.g., S6), fresh-water inputs from northern margins of the EM were also important (Gallego-Torres et al., 2007a). Large fresh-water inputs increased surface-water buoyancy and created a strong halocline, which decreased or even stop vertical mixing and deep-water formation in the Adriatic and Aegean Sea. This led to deep-water restriction and caused an upward migration of the redox chemocline from the sediment-water

interface (SWI) to the water-column, which caused deoxygenation in deep-waters and in intermediate-waters due to an expansion of the Oxygen Minimum Zones (Zirks et al., 2019).

During sapropel events S1, S5 and S7, sea-level was comparable to the present sea-level, fluctuating just a few meters (<20 m below or above the present sea-level), but during cold sapropel events S6 and S8, large ice volumes trapped in the poles and continental glaciers led to a lower sea-level, >60 m below the actual level (Fig. 2) (Grant et al., 2014; Rohling et al., 2014; Sainz de Murieta et al., 2021).

3. Geochemical palaeoceanographic frameworks

The reconstruction of chemical and physical conditions in the water-column during ancient deoxygenation events is not always straightforward from a direct interpretation of geochemical data. In this regard, empirical conceptual models based on geochemical patterns allow to use modern marine restricted settings as analogues hydrogeographic scenarios to the different sapropel events in EM. This can help to establish a wide spectrum of palaeoenvironmental and palaeohydrographic information, such as, robust differentiation between restricted and unrestricted settings, redox conditions in the water-column, stability of the chemocline, and degree of bottom-water restriction (Algeo and Lyons, 2006; Algeo et al., 2007; Algeo and Maynard, 2008; McArthur et al., 2008; Algeo and Tribovillard, 2009; Algeo et al., 2011; Tribovillard et al., 2012; Little et al., 2015; Sweere et al., 2016; McArthur, 2019).

Applied theorical palaeoceanographic models rely on the covariation patterns of trace metals and organic carbon empirically obtained from well-studied modern marine systems. The models applied are: (i) the Co_{EF} x Mn_{EF} vs. %Al plot model from Sweere et al. (2016) and modified by McArthur (2019), (ii) the Mo-U covariation plot model from Algeo and Tribovillard (2009), (iii) the Mo-TOC covariation plot model from Algeo and Lyons (2006), and (iv) the $[Mo]_{aq}$ - renewal time model from Algeo et al. (2007).

(i) The Co_{EF} x Mn_{EF} - Al% plot model from Sweere et al. (2016) and modified by McArthur (2019) allows to discriminate between restricted and unrestricted marine settings. The established Co_{EF} x Mn_{EF} threshold between restricted and unrestricted marine settings is 0.4, which was empirically determined by McArthur (2019). The limitation of this model is that it can only discriminate between extreme hydrographic scenarios, strong restriction or enhanced upwelling.

(ii) The Mo-U covariation plot model from Algeo and Tribovillard (2009) is a powerful tool to evaluate benthic redox conditions, stability of the chemocline, and the intensity of particulate shuttling and its influence on trace metals burial fluxes. The intensity of particulate shuttling in marine basins is obtained by the fact that the transfer of molybdenum (Mo) from the water-column to the sediments is boosted by particulate shuttling, unlike uranium (U), which is not influenced by this process (Tribovillard et al., 2006, 2012). The preferential transfer to the sediments of Mo over U due to particulate shuttling, allows Mo-U covariation plot patterns to assess the intensity of particulate shuttling and its influence on Mo burial fluxes in ancient marine settings (Berrang and Grill, 1974; Helz et al., 1996; Morford et al., 2005; Algeo and Tribovillard, 2009; Algeo et al., 2011; Tribovillard et al., 2012; Scholz et al., 2017; Scholz, 2018; Chiu et al., 2022).

The assessment of redox conditions using the Mo-U plot model is not straightforward for restricted marine settings due to the "basin reservoir effect". The basin reservoir effect implies restricted trace metal resupply during water stagnation, which in turn drawdowns trace metals concentrations in bottom-waters and limits Mo and U authigenic uptake by seafloor sediments. However, the Mo/U trends observed in modern restricted marine settings allow to infer palaeo redox conditions and other parameters, such as, stability of the chemocline and intensity of the basin reservoir effect (Jacobs et al., 1985; Crusius et al., 1996; Algeo and Tribovillard, 2009; Paul et al., 2023).

(iii) The Mo-TOC plot model from Algeo and Lyons (2006) is a particularly helpful tool for establishing a qualitative degree of water-mass restriction in ancient marine systems with oxygen-depleted conditions (Algeo and Rowe, 2012). This conceptual model is supported by the fact that during restricted and oxygen-depleted conditions, Mo is scavenged from seawater into the underlying sediments by authigenic uptake (Bertine and Turekian, 1973; Tribovillard et al., 2006). This triggers Mo depletion, mainly in bottom-waters, until a future deep-water renewal event resupplies Mo to the bottom-waters. Hence, if restriction is intermittent and frequent deep-water renewal occurs, Mo is efficiently resupplied to deep-waters, which is evidenced as high Mo-TOC regression slope values. However, if deep-water restriction is more stable, the renewal of deep-waters decreases and euxinia becomes more recurrent and perennial. This causes a reduction of Mo resupply to the water-column and a more intense basin reservoir effect, which translates into lower Mo-TOC regression slope values (Algeo and Lyons, 2006; McArthur, 2019).

(iv) The $[Mo]_{aq}$-renewal time model from Algeo et al. (2007), which derives from the Mo-TOC plot model from Algeo and Lyons (2006), is a useful model to qualitatively estimate deep-water renewal frequency in ancient marine system. In modern marine restricted settings, aqueous Mo concentration ($[Mo]_{aq}$) and renewal time of bottom-waters have a linear relationship. Therefore, these parameters can be estimated (qualitatively) in ancient settings using a Mo-TOC regression slope (m) obtained from varied modern marine restricted settings (Black Sea, Framvaren Fjord, Cariaco Basin and Saanich Inlet). Consequently, qualitative bottom-water Mo concentration and renewal frequency are obtained for each sapropel event, at the three EM locations (i.e., Ionian Basin, Mediterranean Ridge and Eratosthenes Seamount), by plotting each sapropel m on the abscissa axis of the model. This conceptual model classifies sapropels as black shales categories. It is worth emphasizing that only qualitative estimation of deep-water renewal frequency can be achieved with this model. Marine settings tend to have different redox thresholds and trace metals dynamics due to different hydrogeographic factors (e.g., basin size, seafloor morphology and water-depth) and sedimentation rates. These factors limit a straightforward correlation between ancient and modern settings for the quantitative determination of deep-water renewal times (y) and $[Mo]_{aq}$ during sapropel events based on Mo-TOC covariation patterns (Liu and Algeo, 2020).

4. Materials and methods

4.1. Core description, sampling and chronology

Three ODP Leg 160 sites (964, 966 and 969) were selected in a transect across the EM in order to represent different oceanographic regimes and water-depths. Background sediments of the studied core sediments are principally composed by nannofossil clay, clayey nannofossil ooze and nannofossil ooze, varying in colour from brownish to more greenish and grayish (Emeis et al., 1996). Site 964 (36°15.623′N, 17°45.000′E) is located at the Ionian Basin and represents the deepest marine setting with a water-depth of 3658 m (Figs. 1 and 2). This location is principally influenced by ADW and Western Mediterranean (WM) water masses. Site 966 (33°47.765′N, 32°42.090′E) is situated near the northern margin of the plateau area of the Eratosthenes Seamount, which represents a shallow pelagic setting with a water-depth of 940 m. This site offers the opportunity to evaluate the redox evolution and bottom-water restriction at a shallower water-depth. Site 969 (33°50.399′N, 24°53.065′E) has a water-depth of 2200 m. It is situated on the Mediterranean Ridge, and represents the centermost location of the EM, mainly influenced by the EMDW and the LIW (Emeis et al., 1996; Rohling et al., 2015) (Figs. 1 and 2).

The five selected sapropels represent different environmental conditions and African monsoon intensities, and were deposited from the Middle Pleistocene to the Holocene. Their onset and termination ages have been previously established: S1: 10.5–6.1 ka (MIS 1), S5: 128.5–121.3 ka (MIS 5e), S6: 178.5–165.5 ka (MIS 6d), S7: 198.5–191.9 ka (MIS 7a), and S8: 224.1–209.5 ka (MIS 7c-7d) (Ziegler et al., 2010;

Grant et al., 2016). Sapropels S3 (85.8–80.8 ka) and S4 (107.8–101.8 ka) exist in EM sedimentary record but were not the focus of this study (Fig. 2b) (Grant et al., 2016). Sapropels intervals were sampled at 2 cm resolution, including the sapropels and the underlying and overlying sediments, which offers information on non-sapropel deposition and allows to determine the changes that EM hydrographic regime suffered during sapropels onset and termination. Base and top of sapropels were identified using Ba/Al ratio profiles since original TOC content signal is susceptible to be altered during post-depositional oxidation (Fig. 4) (Higgs et al., 1994; van Santvoort et al., 1996; Gallego-Torres et al., 2007a, 2007b, 2010; Rohling et al., 2015).

4.2. Geochemical analysis of sediments

4.2.1. Major and trace elements

Samples were dried and then powdered in an agata mortar. Due to sample size limitation, XRF analysis for major elements quantification was only performed in S1 samples (prepared as fused beads) from Site

(a)

Sapropel	i-cycle	Age (ka)	Site	Values	TOC%	U EF	Mo EF	Co EF	Mn EF
S1	2	10.5-6.1	964	Mean	1.04	2.7	20.2	2.2	2.3
				Maximum	2.90	5.3	55.9	4.0	6.3
			969	Mean	1.13	3.0	42.7	3.5	15.5
				Maximum	2.81	5.1	147.9	4.5	93.0
			966	Mean	0.53	1.5	7.5	2.2	6.7
				Maximum	1.23	3.2	12.3	2.6	13.5
S5	12	128.3-121.5	964	Mean	4.10	12.7	120.2	3.4	1.4
				Maximum	7.34	23.8	227.3	5.5	2.1
			969	Mean	5.05	42.9	331.6	4.8	2.8
				Maximum	8.45	77.8	703.0	8.5	5.4
			966	Mean	2.57	6.3	87.7	3.3	1.4
				Maximum	5.85	10.1	203.6	5.5	2.4
S6	16	178.5-165.5	964	Mean	2.05	7.7	218.9	2.6	2.0
				Maximum	5.17	10.9	465.0	3.8	2.8
			969	Mean	1.87	13.2	168.8	4.0	3.4
				Maximum	5.90	35.1	676.5	10.2	5.7
			966	Mean	1.16	8.1	54.9	2.9	1.8
				Maximum	2.36	20.7	161.0	5.0	3.1
S7	18	198.5-191.9	964	Mean	3.91	6.7	100.3	2.9	1.5
				Maximum	6.74	12.7	158.8	4.5	2.0
			969	Mean	3.75	24.5	233.1	4.3	2.4
				Maximum	8.23	68.2	670.3	8.0	3.8
			966	Mean	1.60	4.2	43.0	2.4	1.0
				Maximum	3.43	5.8	121.4	3.5	1.2
S8	22	224.1-209.9	964	Mean	1.49	4.7	83.3	2.6	1.8
				Maximum	3.66	7.5	170.5	5.4	5.5
			969	Mean	1.05	8.9	54.5	4.1	7.3
				Maximum	2.55	15.5	178.5	8.3	19.1
			966	Mean	1.06	3.2	19.5	2.8	1.5
				Maximum	2.21	5.3	45.8	4.0	2.5

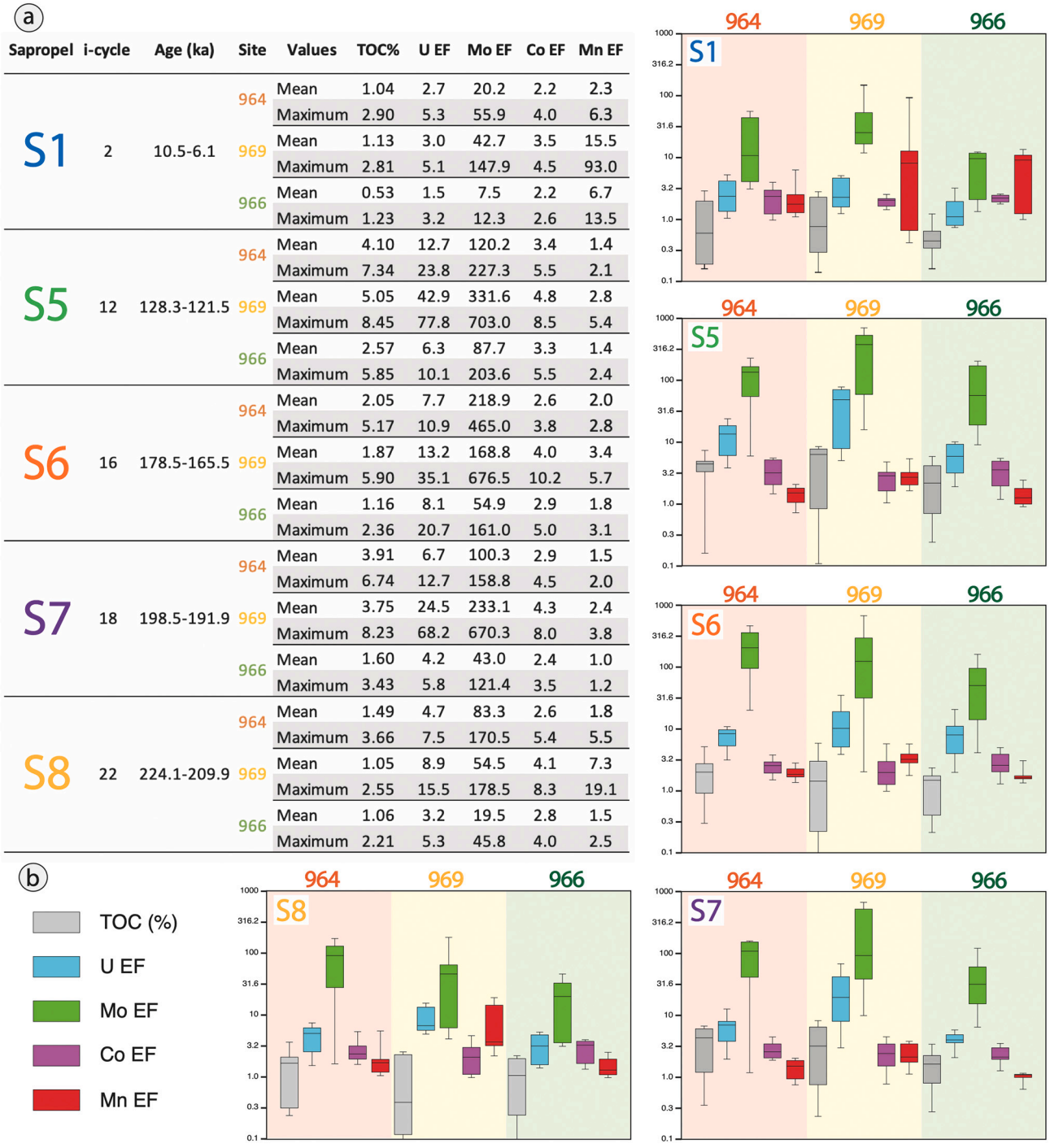

Fig. 3. (a) Table showing mean and maximum values of TOC%, Mo concentration (ppm) and EFs of Mo, U, Co and Mn in each sapropel at the three EM locations. (b) Box-whisker plots showing a comparison between sites for the different sapropels. The box represents the inter-quartile range, the line in the box represents the median and the whiskers represent the 5th and 95th percentiles. Trace metal enrichments and TOC% are shown in $\log_{10}$ scale. Insolation cycles (i-cycles) and time intervals of each sapropel are also indicated. S1 and S5 ages from Grant et al. (2016) and S6, S7 and S8 ages from (Ziegler et al. (2010).

964. XRF was carried out at Instituto Andaluz de Ciencias de la Tierra (IACT), with a S4 Pioneer from BRUKER, equipped with a 4 kW wavelength dispersive X-ray fluorescence spectrometer (WDXRF) and a Rh anode X-ray tube (60 kV, 150 mA). XRF precision was better than ±0.3% for major elements. In the rest of samples, major elements were measured with an ICP-OES Perkin-Elmer Optima 8300 (Dual View) with an autosampler Perkin-Elmer. Certified standards (BR-N, GH, DR-N, UB-N, AGV-N, MAG-1, GS-N, and GA) were measured for element quantification. Trace elements, in all samples, were measured using an ICP-MS NexION 300d (Perkin Elmer) spectrometer using Rh as internal standard. For major elements, ICP-OES precision was better than ±1% and for trace elements ICP-MS precision was better than ±5% for analyte concentrations of 10 ppm (Bea, 1996).

ICP-MS and ICP-OES analyses were carried out at the Scientific Instrumentation Center (CIC, University of Granada) and measured using the same solutions, which were prepared in batches of 25 to 30 samples, and analytical blanks were introduced in each sample batch. Solutions were prepared with 0,1 g of powdered sample in Teflon vessels, where successive acid digestions using HNO_3 (ultra-pure with a 69% concentration) and HF (48% concentration) were performed at 130 °C until evaporation. A final acid digestion with HNO_3 and water at 80 °C for 1 h was also performed. Subsequently, the digested samples were diluted with Milli-Q water in 100 ml volumetric flasks (Bea, 1996).

4.2.2. Organic matter content

TOC content was measured by the Rock-Eval pyrolysis method, at the Institute of Earth Sciences (ISTE) of the University of Lausanne (UNIL). The Rock-Eval pyrolysis method consisted of a programmed temperature heating (from 200 °C to 850 °C, in successive steps), in a pyrolysis oven with an inert atmosphere (N_2). TOC% is calculated from the obtained thermograms using the following equation; TOC% = Pyrolysed Carbon (wt%) + Residual Carbon (wt%). Samples were calibrated using the IFP160000 standard with an instrumental precision of <0.1 wt% for TOC (Lafargue et al., 1998; Behar et al., 2001; Ordoñez et al., 2019).

5. Results

Results of the main geochemical parameters used for the construction of the palaeoceanographic conceptual models (TOC (%), Mo (ppm), U_{EF}, Mo_{EF}, Co_{EF} and Mn_{EF}) are presented in Figs. 3 and 4. Trace metals Enrichment Factors (EFs) were obtained by applying the following equation: $TM_{EF} = (TM/Al)_{sample}/(TM/Al)_{reference}$, with the post-Archean Australian shale (PAAS) values from Taylor and McLennan (1995) as reference values to enable comparability with other studies, even when local background TM/Al values may be preferred over bibliographic reference values (Paul et al., 2023). The largest Mo and U enrichments are recognized in the Mediterranean Ridge (Site 969), followed by the Ionian Basin (Site 964), and the lowest Mo and U enrichments lowest at Eratosthenes Seamount (Site 966). Sapropels S5, S6 S7 are the sapropels most enriched in Mo and U (Figs. 3 and 4) and have similar Mo concentrations. Sapropels S5 and S7 are more enriched in U than sapropel S6, while S6 is more enriched in Mo. S1 and S8 register the lowest U and Mo concentrations among all the studied sapropels, where S1 has the lowest U and Mo concentrations, but the highest Mn concentrations, especially at the Mediterranean Ridge. Co has similar concentrations in the three locations and in the five sapropels (mean Co_{EF} from 2 to 4.8), though it is slightly higher at the Mediterranean Ridge (Figs. 3 and 4).

Regarding the TOC content, it is higher in the Ionian Basin and Mediterranean Ridge than in the Eratosthenes Seamount. S1 and S8 exhibit the lowest TOC content (below 1.5 mean TOC%), followed by S6 (below 2.1 mean TOC%). S5 and S7 present the highest TOC content, reaching up to 5% in S5 at the Mediterranean Ridge (Figs. 3 and 4; Supplementary Material).

Fig. 4 shows the Mo, U and TOC enrichments in sapropels layers. Some Mo and U enrichment are associated to post-depositional processes and remobilization. (i) Downward oxidation caused Mo remobilization and subsequent Mo enrichments in the oxidation front in S1 at the Mediterranean Ridge and Eratosthenes Seamount (Fillippidi and De Lange, 2019), (ii) strong downward sulfidation caused Mo enrichments below S1 at the Mediterranean Ridge (Passier et al., 1996), and (iii) intense reoxygenation during reventilation caused downward migration of U enrichment in S1 at the Mediterranean Ridge and Eratosthenes Seamount (Zheng et al., 2002; Tribovillard et al., 2006) (Fig. 4). Consequently, sapropels strongly affected by these post-depositional processes or with weak Mo and TOC enrichments due to weak oxygen depletion, generated unreliable Mo-TOC regression slopes. For these reasons, the degree of deep-water restriction using the Mo-TOC regression slopes will not be assessed for S1 at Eratosthenes Seamount and the Mediterranean Ridge, and for S8 and S6 at Eratosthenes Seamount.

6. Discussion

The Ionian Basin, Mediterranean Ridge and Eratosthenes Seamount represent very different hydrogeographic regimes. However, almost all sapropel values and non-sapropel values, at the three locations, fall in the "restricted" area of the Co_{EF} x Mn_{EF} - Al% plot model, even Eratosthenes Seamount, the shallowest location and the most susceptible to experience lateral advection (Fig. 5c). Therefore, this model supports that EM sub-basins can be considered restricted marine settings since they have a similar behavior to the modern Baltic Sea or Black Sea in the Co_{EF} x Mn_{EF} - Al% plot model (McArthur, 2019). In these restricted settings, Co and Mn cannot escape the "closed" system due to reduced water-column circulation and enhanced trapping efficiency (Sweere et al., 2016; McArthur, 2019). Consequently, Co and Mn are permanently fixed in the sediments via redox cycling, where Co is typically fixed in pyrite (FeS) or as its own sulfide (CoS), while Mn is typically fixed as rhodochrosite ($MnCO_3$) or as Mn-oxyhydroxides depending on the redox conditions (Calvert and Pedersen, 1996, 2007; Tribovillard et al., 2006; Dellwig et al., 2010; Böttcher et al., 2012). Moreover, the data suggest that Co_{EF} x Mn_{EF} - Al% plot model responds better to regional than to local factors and does not discriminate sapropel from non-sapropel sediments since their values overlap (Fig. 5).

6.1. Particulate shuttling and degree of oxygen depletion

In general terms, the Mo_{EF}-U_{EF} covariation patterns observed in EM during sapropel deposition indicate intense particulate shuttling, similar to the observed in the present Cariaco Basin. However, according to the Mo_{EF}-U_{EF} covariation patterns, each sapropel event presents specific hydrographic features. S5, at the Ionian Basin, and S5 and S7 at the Mediterranean Ridge, show deviating values from the rest of the sapropels ($U_{EFs} > 20$ and $Mo_{EFs} > 200$), which converge with the redox trend recorded in unrestricted marine settings (Fig. 6). According to Tribovillard et al. (2012), in restricted marine settings this pattern is indicative of a restricted water-column with strong and stable euxinic conditions and intense particulate shuttling. The lower Mo/U ratios suggests progressive Mo drawdown due to poor Mo resupply to bottom-waters and the higher authigenic U concentrations in comparison to the rest of sapropels suggesting higher U fixation rate due to stronger and more stable anoxia/euxinia. Therefore, S5 and S7 deposition in EM occurred under strong and stable deep-water euxinia, as is also demonstrated by the covariation patterns of Fe, U and Mo isotopes in S5 and S7 (Andersen et al., 2018; Benkovitz et al., 2020; Sweere et al., 2021; Chiu et al., 2022).

Conversely, S1 and S8 have the lowest authigenic U and Mo concentrations, suggesting the weakest particulate shuttling activity and oxygen depletion at the three sites, where suboxic conditions in the water-column seem to have ruled during most of their deposition (Fig. 6). Nevertheless, the Mo enrichment by itself in S1 and S8, demonstrate that during their deposition sulfidic conditions were reached, especially in EM deepest settings. This goes in agreement with

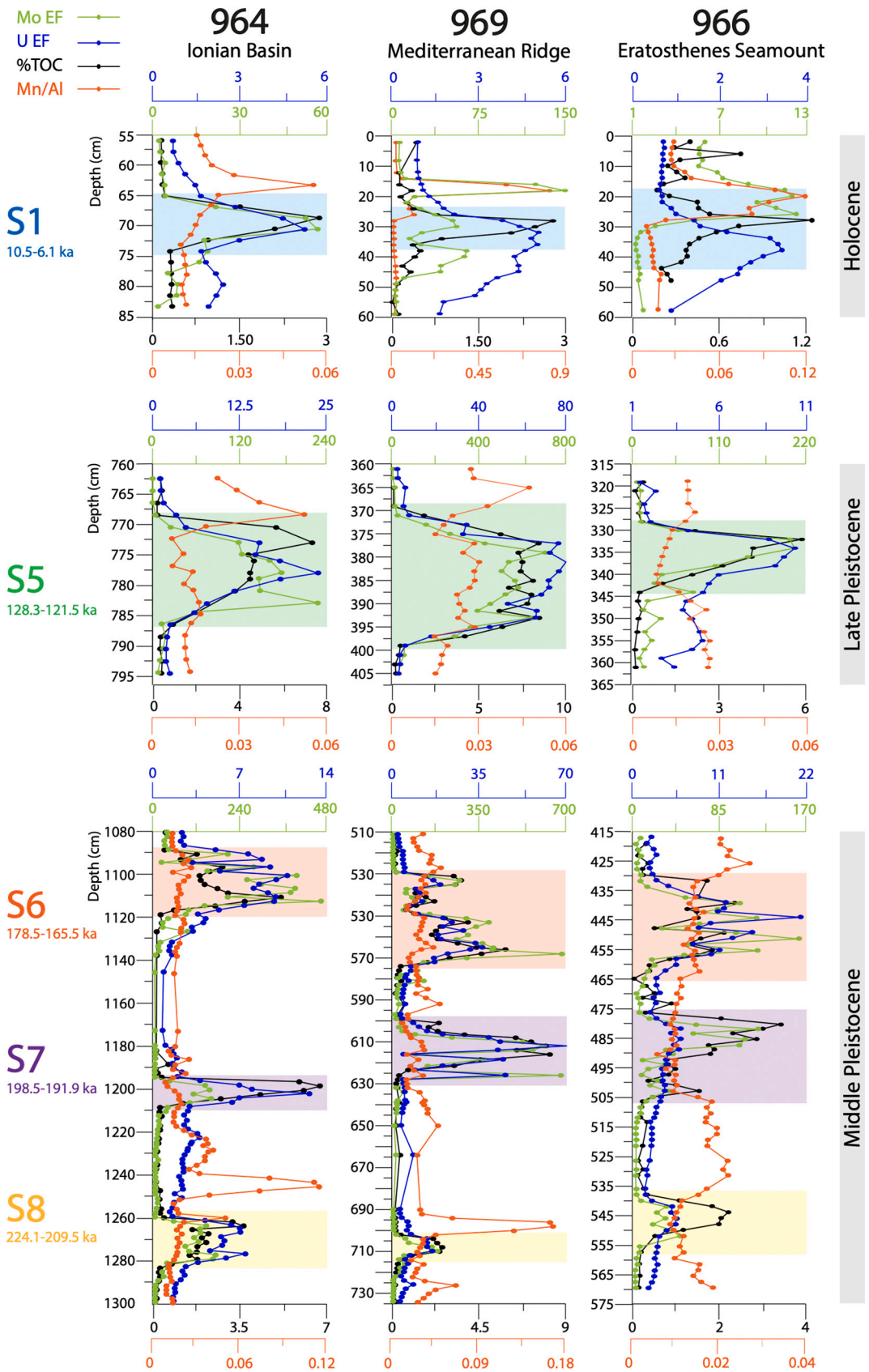

Fig. 4. Chemostratigraphic figure showing Mo_{EF}, U_{EF}, TOC% and Mn/Al plotted in vertical dimension for sapropels S1, S5, S6, S7 and S8 from the Ionian Basin, Mediterranean Ridge and Eratosthenes Seamount. For sapropels time intervals references see Fig. 3.

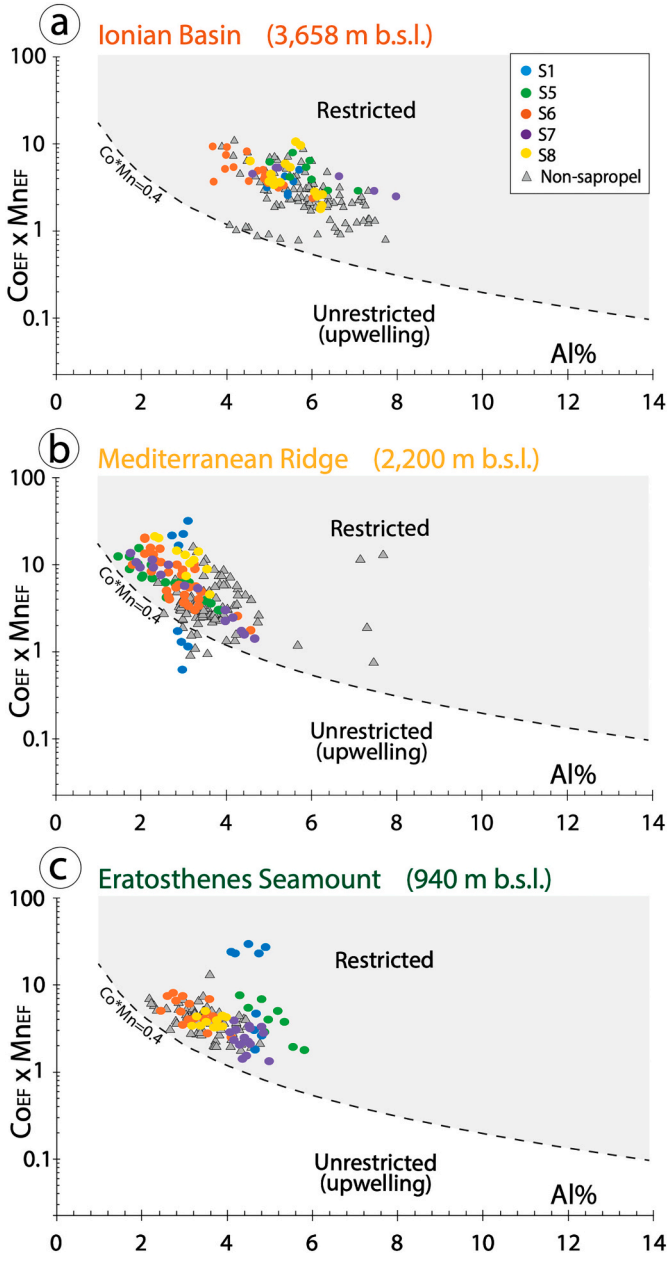

Fig. 5. The Co_{EF} x Mn_{EF} vs. Al% conceptual model of Sweere et al. (2016) and modified by McArthur (2019) used to interpret depositional environments (restricted vs. unrestricted) at each location. Field divider (dashed line) is Co_{EF} x Mn_{EF} = 0.4. Sapropels and non-sapropel data are illustrated with different colors. (a) Ionian Basin (S1 n = 8, S5 n = 10, S6 n = 16, S7 n = 7, S8 n = 16, non-sapropel n = 108), (b) Mediterranean Ridge (S1 n = 9, S5 n = 20, S6 n = 34, S7 n = 15, S8 n = 11, non-sapropel n = 96), and (c) Eratosthenes Seamount (S1 n = 9, S5 n = 9, S6 n = 20, S7 n = 16, S8 n = 11, non-sapropel n = 65).

recent studies that used Fe, U and Mo isotopes to support that sulfidic conditions were reached during S1 deposition (Azrieli-Tal et al., 2014; Matthews et al., 2017; Andersen et al., 2020; Sweere et al., 2021). Furthermore, S1 at the three locations and S8 at the Ionian Basin and Mediterranean Ridge, show abrupt "marker beds" evidenced by Mn peaks on the top of the sapropels (Fillippidi and De Lange, 2019), which in some cases are accompanied with Mo enrichments associated with Mn-oxyhydroxides (e.g., S1) (Figs. 4 and 5). This demonstrates that strong and rapid bottom-water ventilation occurred in EM below 900 m after S1 and below 2000 m after S8.

S6 is the most influenced sapropel by particulate shuttling. Extremely high Mo concentrations (Mo_{EF} > 200) and low U concentrations (U_{EF} > 25) are indicative of marine systems with frequent fluctuations of the chemocline depth (from below the SWI to the water-column and vice versa) and high-frequency temporal redox variations (i.e., unstable bottom aoxia/euxinia), due to an unstable hydrographic regime with intense particulate shuttling and frequent deep-water renewal (Figs. 8 and 9) (Algeo and Lyons, 2006; Algeo and Tribovillard, 2009; Scholz et al., 2017). The fluctuating chemocline and the frequent deep-water renewal during S6 deposition vastly resupplied trace metals to bottom-waters and led to "Mo burial pumps" (Algeo and Tribovillard, 2009) (Figs. 6 and 9).

The principal source of Mo for authigenic uptake in EM is seawater (Nijenhuis et al., 1998), therefore, the high Mo concentrations and the palaeoceanographic models suggest that Mo was not depleted in EM water-masses during S6 deposition. This supports increased Mo resupply and high Mo concentrations in EM bottom-waters during S6, despite the lower sea-level and shallower basin sill between WM and EM, i.e., the Strait of Sicily, which had a depth of 250 m (Fig. 9). This is probably associated to the fact that surface-water exchange between WM and EM was vigorous during S6 due to increased low-density Atlantic inflow into the Mediterranean, fueled by melted Atlantic ice sheets (Sierro and Andersen, 2022). Consequently, WM and EM water-mass exchange efficiently resupplied Mo and other trace metals to EM, where they were supplied to bottom-waters by intermittent deep-water formation during cold periods. Nevertheless, the low-density surface-waters that reached EM, probably weakened deep-water formation in the Adriatic Sea and Aegean Sea and promoted brief bottom-water stagnation and euxinia.

However, according to the applied theorical models, Mo was progressively depleted in EM water-masses during S5 and S7. This supports enhanced basin reservoir effect and weak surface-water exchange between EM and WM during S5 and S7 deposition, where Mo uptake rate by seafloor sediments was higher than the Mo input from WM, causing a progressive Mo drawdown in EM deep water-masses (Benkovitz et al., 2020; Sweere et al., 2021). During S1 and S8, Mo was not depleted in EM water-masses, probably because oxygen depletion was not strong enough to cause Mo burial rates to surpass Mo resupply in EM bottom-waters (Fig. 6). In the case of S8, water-mass exchange between EM and WM was probably enhanced (i.e., higher Mo resupply) since it was deposited during a glacial period (i.e., colder temperatures), as occurred during S6 (Sierro and Andersen, 2022).

In respect to differences between locations, the Mediterranean Ridge and the Ionian Basin developed stronger oxygen depletion and more intense particulate shuttling (higher Mo and U concentrations) than Eratosthenes Seamount during sapropel deposition. However, the Mediterranean Ridge sediments have higher U concentrations than Ionian Basin sediments, indicating that the Mediterranean Ridge (at least below 2200 m) suffered stronger oxygen depletion than the Ionian Abyssal Plain. Weaker oxygen depletion at the Ionian Basin than at the Mediterranean Ridge, is probably due to its hydrogeographic location (i.e., local factors). The Ionian Abyssal Plain appears to be more responsive to the formation of EM deep-water masses (e.g., ADW Outflow and EMDW), which prevent it from experiencing stronger bottom-water deoxygenation despite being the location that develops earlier oxygen depletion. Eratosthenes seamount is the shallowest location (intermediate waters), hence, has a smaller overlying water-column for trace metals to be scavenged (i.e., smaller trace metals reservoir) and is more prone to experience bottom-water renewal (Zirks et al., 2019), therefore, it is the location with weaker particulate shuttling and oxygen depletion. However, particulate shuttling was still intense and similar to the modern Cariaco Basin (Fig. 6c).

6.2. *Degree of deep-water restriction*

Mo-TOC regression slopes (m) obtained from modern marine settings with different degrees of deep-water restriction (i.e., Saanich Inlet, Cariaco Basin, Framvaren Fjord and Black), serve as an analogue

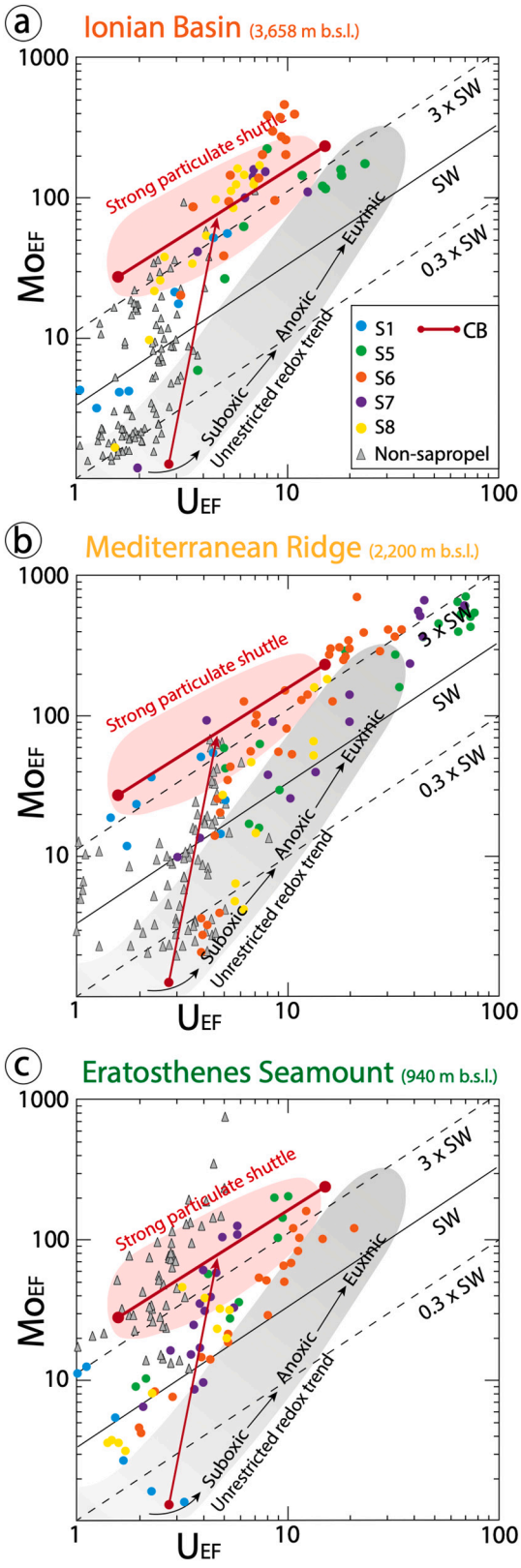

(caption on next column)

Fig. 6. Mo_{EF}-U_{EF} conceptual model from Algeo and Tribovillard (2009). The plot model shows Mo_{EF}/U_{EF} covariation patterns of sapropels at the three locations. Sapropels and non-sapropel data is illustrated with different colors. Diagonal solid line represents seawater (SW) Mo/U molar ratio of ~7.5–7.9 and fractions thereof in dashed lines (3xSW and 0.3xSW). Red solid line: covariant Mo/U trend in modern Cariaco Basin (CB). Gray shaded area: redox trend of unrestricted marine (UM) settings. Red shaded area: intense particulate shuttling. Mo(ppm) - U(ppm) correlation coefficients at each location: (a) Ionian Basin ($r = +0.69$; $p(\alpha) < 0.01$; $n = 165$), (b) Mediterranean Ridge ($r = +0.85$; $p(\alpha) < 0.01$; $n = 159$), and (c) Eratosthenes Seamount ($r = +0.58$; $p(\alpha) < 0.01$; $n = 132$). (For interpretation of the references to colour in this figure legend, the reader is referred to the web version of this article.)

hydrographic scenario to each sapropel event and allow to estimate a qualitative degree of deep-water restriction. There is congruence for the degree of deep-water restriction at regional scale for each sapropel event. However, local variability in particulate shuttling intensity and degree of bottom-water restriction during sapropel events caused differences in Mo burial fluxes between sites, and subsequent differences in the Mo-TOC regression slopes (Algeo and Lyons, 2006; Liu and Algeo, 2020). In this sense, the Mo-TOC regression slopes are more sensitive to local hydrographic factors than the Co_{EF} x Mn_{EF} vs. Al% plot model, which enables to mark out differences in the degree of deep-water restriction between sites during the deposition of each sapropel.

During each sapropel event, deep-water masses were restricted to different degrees. S1 slope at the Ionian Basin ($m \sim 11.3 \pm 1.3$) suggests a degree of deep-water restriction similar to the modern Framvaren Fjord. Hence, despite weak African monsoon intensity and low freshwater input during S1 deposition (Rohling et al., 2015; Gallego-Torres et al., 2007a), S1 developed strong deep-water restriction and low-frequency temporal redox variations at the deepest EM settings (Figs. 7a and 8). Conversely, S1 did not develop stable bottom-water restriction at shallower sites than the abyssal Ionian Basin (e.g., Mediterranean Ridge or Eratosthenes Seamount). Consequently, we can state that shallower sites than the Ionian Basin are less prone to develop stable deep-water restriction and subsequent bottom-water euxinia. This agrees with Fillippidi and De Lange (2019) who state that S1 deposition occurred under variable redox conditions at different water-depths. However, the results also suggest that once stable deep-water restriction is established at the Mediterranean Ridge, it develops stronger oxygen depletion (i.e., higher U enrichments) than the Ionian Basin, as occurred during S5, S6, S7 and S8 (Fig. 9).

S5 and S7 show the lowest Mo-TOC slope values (Fig. 7), therefore, represent sapropel events with the highest degree of water-mass restriction among the studied sapropels with similar hydrographic regime as that in the Framvaren Fjord ($m \sim 9 \pm 2$) or Black Sea ($m \sim 4.5 \pm 1$), as also previously suggested (Gallego-Torres et al., 2007a; Rohling et al., 2015; Andersen et al., 2018; Benkovitz et al., 2020; Sweere et al., 2021; Chiu et al., 2022). This means that during S5 and S7 deposition, deep-water restriction in EM was stronger and more perennial than during S1, S6 and S8. This agrees with the Mo isotope results from Sweere et al. (2021), which indicate that among the studied sapropels in this study, S5 and S7 are the sapropel events with the strongest oxygen depletion (comparable to the modern Black Sea), followed by S6, S8 and S1, respectively. This is linked to the climatic conditions that ruled S5 and S7 events, which were characterized by exceptionally strong African monsoons that drastically increased fresh-water input and caused severe surface-water freshening and sluggish deep-water circulation (Nolet and Corliss, 1990; Casford et al., 2003; Capotondi et al., 2006; Gallego-Torres et al., 2007a; Marino et al., 2007; Osborne et al., 2010; Rohling et al., 2015; Benkovitz et al., 2020).

S5 and S7 seem to be the only sapropel events that developed perennial anoxia and stable bottom-water restriction and euxinia above 1000 m below sea-level (i.e., in intermediate-waters), since they are the only sapropels that reached relatively high Mo concentrations (between 50 and 100 ppm) at Eratosthenes Seamount. At this location, Mo-TOC

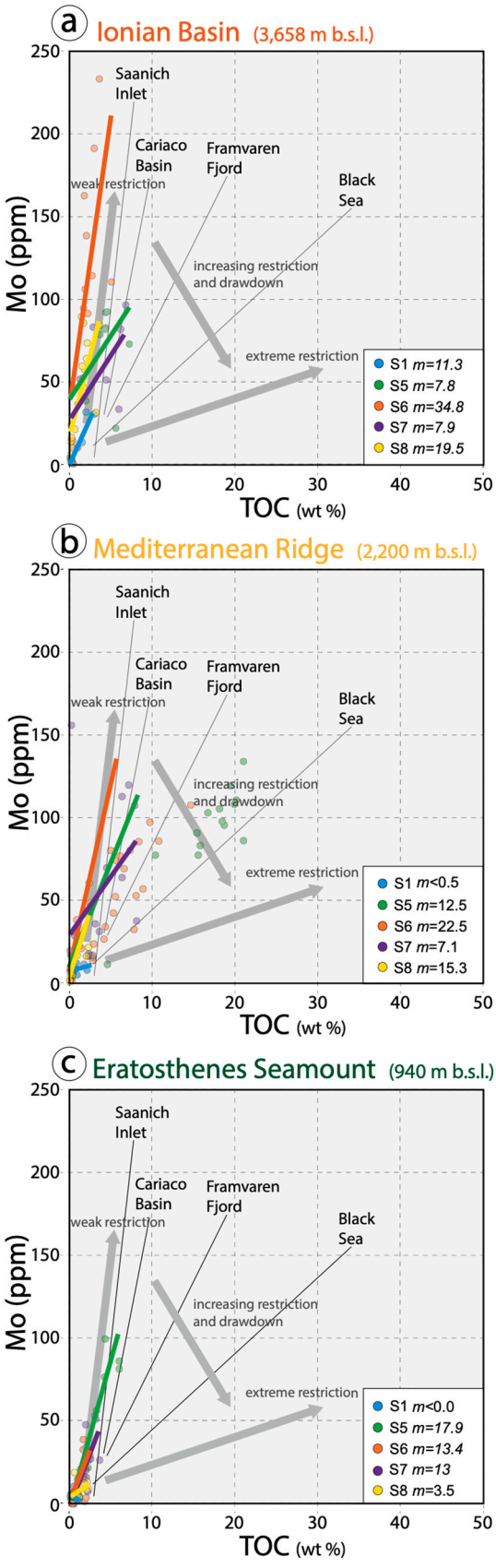

(caption on next column)

Fig. 7. Mo-TOC conceptual model from Algeo and Lyons (2006) applied to studied sapropels at each location. Regression slopes from different modern anoxic silled-basins are shown on the conceptual model as modern analogues to the sapropels (Saanich Inlet, $m \sim 45 \pm 5$; Cariaco Basin, $m \sim 25 \pm 5$; Framvaren Fjord, $m \sim 9 \pm 2$ and Black Sea, $m \sim 4.5 \pm 1$). Gray arrows suggest degree of water-mass restriction. Slopes and slope values (m) of each sapropel are indicated in the figure. Mo(ppm) - TOC% correlation coefficients per location: (a) Ionian Basin ($r = +0.65$; $p(\alpha) < 0.01$; $n = 112$), (b) Mediterranean Ridge ($r = +0.80$; $p(\alpha) < 0.01$; $n = 121$), and (c) Eratosthenes Seamount ($r = +0.71$; $p(\alpha) < 0.01$; $n = 115$);. Detailed Mo-TOC statistic parameters of each sapropel in Fig. 8.

slopes ($m \sim 17.9 \pm 2.6$; $m \sim 13 \pm 3.2$ respectively; Fig. 7c) fall between the Cariaco Basin slope ($m \sim 25 \pm 5$) and the Framvaren Fjord slope, supporting moderate to strong bottom-water restriction and oxygen depletion in intermediate water-masses during their deposition.

At the Ionian Basin and Mediterranean Ridge, S6 and S8 have the highest slope values (Fig. 7), therefore experienced the weakest deep-water restriction (i.e., the most frequent deep-water renewal) and had a similar degree of deep-water restriction as that in Saanich Inlet or Cariaco Basin, respectively. This could be linked to the fact that both sapropels were deposited under cold temperatures that promoted more frequent deep-water formation, which prevented stable euxinia in EM bottom-waters (Figs. 9c). However, S6 Mo-TOC slope at Eratosthenes Seamount ($m \sim 13.6 \pm 3.2$) suggests the most restricted scenario among the three locations, being close to a Framvaren Fjord scenario (Fig. 7). Nevertheless, Mo concentrations in sapropel S6 at this location are not high enough to make its respective Mo-TOC slope reliable to state this. Moreover, this statement would go in disagreement with the other two locations that indicate frequent deep-water renewal and with the lower water-depth, normally related to weaker bottom-water restriction.

6.3. *Deep-water renewal frequency and* $[Mo]_{aq}$

A qualitative deep-water renewal frequency is obtained for the sapropel layers at each location based on a comparison between Mo-TOC regression slopes (m) obtained from modern marine restricted settings. Empirical data suggest that high m values are characteristic of marine settings with weak deep-water restriction, frequent deep-water renewal, high Mo concentration in bottom-waters and high-frequency temporal redox variations (e.g., Saanich Inlet or Cariaco Basin), and the opposite for low m values (e.g., Black Sea or Framvaren Fjord). Therefore, modern marine restricted settings serve as analogues to determine more precise palaeohydrographic parameters, such as, qualitative deep-water renewal frequency and deep-water aqueous Mo concentration (Algeo et al., 2007; Little et al., 2015).

S1 deep-water restriction signal was only recognized at the Ionian Basin, probably due to its greater water-depth that allowed rapid bottom-water restriction and deoxygenation (Azrieli-Tal et al., 2014). Therefore, stable euxinia during S1 occurred in the deepest EM settings with stable bottom-water restriction and under high export production areas (Casford et al., 2003). Consequently, the differences in EM settings exposed in the palaeoceanographic conceptual models suggest a limited extent of truly anoxic conditions in space, water-depth and time during S1 deposition due to local hydrogeographic features (Fig. 9a) (Fillippidi and De Lange, 2019).

For most sapropels, the Mo-TOC regression slopes range between 10 and 25, which correspond to intermediate-m black shales, however, some exceptions are observed. S7 and S5 at Mediterranean Ridge and S7 for the Ionian Basin are the only sapropels that fall in the low-m black shales category, indicating the highest deep-water renewal time among the studied sapropels and the lowest aqueous Mo concentrations in bottom-waters. This is in accordance with the high bottom-water renewal time for S5 (1030 + 820/−520 years) obtained from U isotopes by Andersen et al. (2018). Therefore, S5 and S7 were deposited under a stable hydrographic regime with low-frequency redox variations

(a)

Sapropel	Age (ka)	Location	*n*	Median TOC%±1σ	Median Mo(ppm)±1σ	Mo-TOC *m*±1σ (x10-4)	*r2*	*r*	*p*
S1	10.5-6.1	Ionian Basin	8	1.1±0.6	6±13	11.3±1.3	0.93	0.96	<0.01
		Mediterranean Ridge	9	0.8±1.1	8±12	<0.5	-	-	-
		Eratosthenes Seamount	9	0.5±0.3	5±2	<0.0	-	-	-
S5	128.3-121-5	Ionian Basin	10	4.5±2.1	80±40	7.8±6.7	0.15	0.53	0.14
		Mediterranean Ridge	20	6.4±3.3	85±42	12.5±0.9	0.92	0.96	<0.01
		Eratosthenes Seamount	9	2.17±1.9	26±37	17.9±2.6	0.88	0.94	<0.01
S6	178.5-165.5	Ionian Basin	16	2.01±1.3	100±68	34.8±10.3	0.45	0.67	<0.01
		Mediterranean Ridge	34	1.7±1.6	33±42	22.2±2.5	0.7	0.83	<0.01
		Eratosthenes Seamount	20	1.4±0.7	17±13	<0.0	-	-	-
S7	198.5-191.9	Ionian Basin	7	4.3±2.5	52±33	7.9±4.7	0.36	0.6	0.16
		Mediterranean Ridge	15	3.2±2.9	36±48	7.1±4.2	0.18	0.43	<0.01
		Eratosthenes Seamount	16	1.6±0.1	14±17	<0.0	-	-	-
S8	224.1-209.5	Ionian Basin	16	1.7±1.1	50±30	19.5±5.3	0.49	0.7	<0.01
		Mediterranean Ridge	11	0.39±1.1	16±20	15.3±3.6	0.67	0.82	<0.01
		Eratosthenes Seamount	11	1.07±0.8	8±6	<0.0	-	-	-

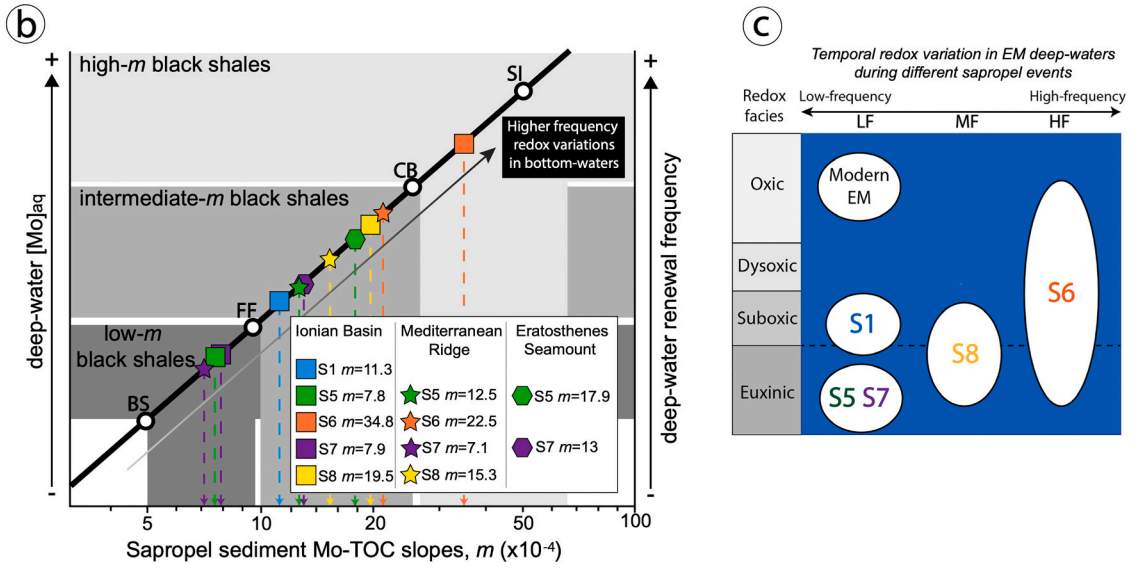

Fig. 8. (a) Table showing Mo-TOC statistic parameters of each sapropel at the three locations. (b) $[Mo]_{aq}$-deep-water renewal time model from Algeo et al. (2007). This conceptual model allows qualitative deep-water renewal frequency and deep-water [Mo]aq during deposition of sapropels. Sapropels are categorized in "low-*m* black shales" ($m < 10$), "intermediate-*m* black shales" ($10 < m < 25$), and "high-*m* black shales" ($m < 25$). Most study sapropels fall in category of "intermediate-*m* black shales". (c) Modified conceptual redox classification scheme from Algeo and Li (2020) based on modern marine systems, where sapropel events are classified by the frequency of temporal redox variations, which can be low-frequency (LF), mid-frequency (MF), or high-frequency (HF). Modern analogues: BS: Black Sea, CB: Cariaco Basin, FF: Framvaren Fjord, and SI: Saanich Inlet. Sites water-depths: Ionian Basin: 3658 m, Mediterranean Ridge: 2200 m, and Eratosthenes Seamount: 940 m. Only sapropels with reliable Mo-TOC slopes were included in this model. For sapropels time intervals references see Fig. 3.

in deep-water masses (Fig. 9b). However, sporadic vertical mixing and associated resupply of trace-metals to bottom-waters could not have been totally absent since both sapropels reach high Mo concentrations in their sediments and only experience Mo depletion during its termination (Fig. 8) (Sweere et al., 2021).

Another aspect that we suggest that should be to taken into consideration is that during stable deep-water stagnation in EM, brines derived from the dissolution of underlying evaporite deposits and mud diapirs can increase salinity in bottom-water masses (Emeis et al., 1996; van Santvoort and de Lange, 1996; Camerlenghi et al., 2019). Therefore, if deep-water masses are not frequently renovated, bottom-water salinity increases, especially in deep abyssal plains where brines tend to accumulate (van Santvoort and de Lange, 1996). Thus, we suggest that during periods of strong and stable water-column stratification, as occurred during S5 and S7 events, upward salinity fluxes from the sediments increased deep-water salinity increase. This in turn created a stronger halocline and pycnocline that inhibited vertical mixing and reinforced stagnation and trace metals depletion in bottom-waters. In contrast, during sapropel events characterized by more frequent deep-water renewal (e.g., S1, S6 and S8), such salinity fluxes did not drastically increase bottom-water salinity since bottom-water masses were reventilated and renewed by vertical mixing during episodes of thermohaline circulation reactivation, preventing trace-metals to suffer strong depletion in bottom-waters (Figs. 9b).

S6 presents the highest *m* values and is the only sapropel that falls into the high-*m* black shales category, suggesting a hydrographic regime with more frequent deep-water renewal and higher concentrations of aqueous Mo in bottom-waters among the studied sapropels (Fig. 8). This may relate to it being deposited during the end of a glacial climatic episode, as S8. Hence, they were deposited under colder temperatures

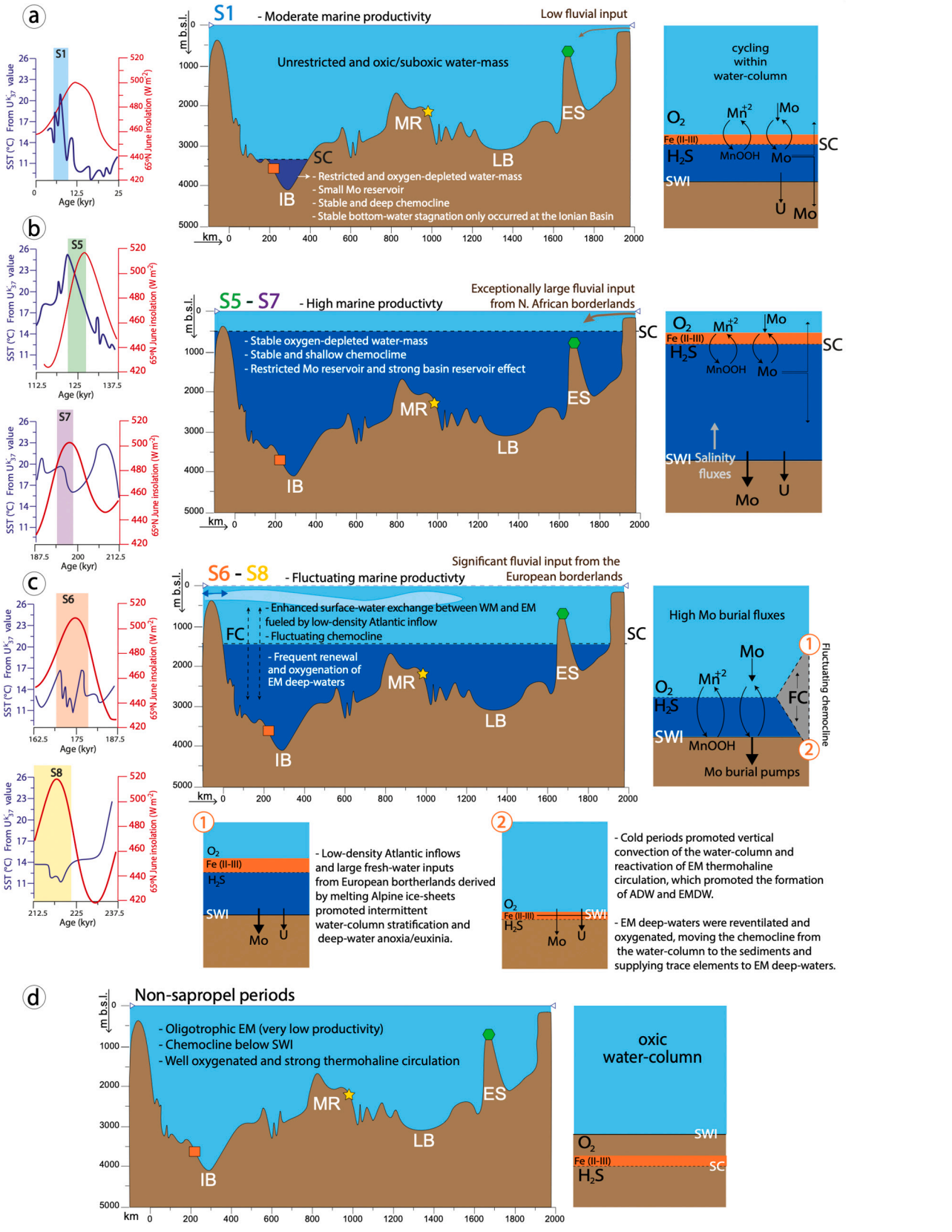

(caption on next page)

Fig. 9. Synthetic and schematic depositional model during the deposition of S1 (a), S5 and S7 (b), S6 and S8 (c), and non-sapropel periods (d) across the EM transect at the three studied locations (Ionian Basin = IB, Mediterranean Ridge = MR and Eratosthenes Seamount = ES in the Levantine Basin = LB). The schemes show the hydrographic and geochemical processes that ruled during each the deposition of each sapropel. The schemes are based on hydrographic schemes from Algeo and Tribovillard (2009) and data obtained from the palaeoceanographic geochemical conceptual models applied in this study. Qualitative productivity rate and relative fluvial inputs from Gallego-Torres et al. (2007a, 2010,). Temperature curve obtained by Emeis et al. (2003) from $U^{K'}_{37}$ (dark blue) at the Mediterranean Ridge and summer insolation curve (red) at 65°N obtained by Laskar et al. (1993) are shown for each sapropel. FC: fluctuating chemocline, SC: stable chemocline, SST: sea surface-temperature, SWI: sediment-water interface. Water-masses: light blue represents oxic conditions and unrestricted water-mass; orange represents anoxic (non-sulfidic) conditions (zones of Fe(III), Mn(IV) and nitrate reduction) and dark blue represents sulfidic conditions (sulfate reduction) and restricted water-mass. Size of arrows reflect relative magnitudes of authigenic Mo and U fluxes to the sediment. For sapropels time intervals references see Fig. 3. (For interpretation of the references to colour in this figure legend, the reader is referred to the web version of this article.)

than the average sapropel and lower sea-level that may have promoted upwelling currents and vertical convection, and subsequently, more frequent thermohaline reactivation and deep-water ventilation (Figs. 9c) (Gallego-Torres et al., 2007a; (Melki et al., 2010; Grant et al., 2014).

However, low-density Atlantic inflow was enhanced during this period, allowing low-density surface-waters to reach EM basin (Sierro and Andersen, 2022). Moreover, during S6 event, fresh-water inputs from northern borderlands (Europe) derived from melted Alpine ice sheets sourced large volumes of fresh-water into Adriatic Sea, which is the location where most EMDW is formed (Ozsoy, 1981; POEM Group, 1992; Lascaratos et al., 1999; Gallego-Torres et al., 2007a). Therefore, the interplay between the aforementioned factors during S6 event weakened EMDW formation, which caused intermittent deep-water restriction and associated intermittent anoxia/euxinia in deep EM settings (Fig. 9c) (Sierro and Andersen, 2022).

EMDW intermittent circulation and enhanced water-mass exchange between EM and WM fluctuated the chemocline position from the water-column to below the SWI during the deposition of S6. This caused high-frequency temporal redox variations in EM deep settings and boosted Mo resupply to bottom-water, leading to higher aqueous Mo concentrations in bottom-waters that ultimately promoted the aforementioned "Mo burial pumps" (Fig. 9c) (Algeo and Tribovillard, 2009). This explains why S6 shows the highest Mo concentrations, even though it is not the sapropel event associated to the strongest euxinia among the studied sapropels (Gallego-Torres et al., 2007a; Rohling et al., 2015; Sweere et al., 2021).

S8 represents a similar scenario to the modern Cariaco Basin, in terms of temporal redox variations and deep-water restriction and chemistry (Fig. 9). S. The frequent deep-water renewal during S8 is associated to the fact that it was deposited during a glacial period, where cold temperatures and dry air masses stimulated more frequent deep-water formation, as occurred during S6. However, S8 has lower Mo and U concentrations (Fig. 6), and higher Mn concentrations than S6, therefore S8 suffered weaker oxygen depletion, weaker surface-water freshening and lower primary productivity (Gallego-Torres et al., 2007a), and probably weaker influence of low-density Atlantic inflow on EM water-column stratification (Fig. 9c).

7. Conclusions

The results obtained from the studied sapropels offer insights into the changes in deep-water circulation and redox conditions that EM experienced during different climate conditions. This offers palaeo-perspectives to modern marine systems that are undergoing oxygen depletion due to the current global warming and anthropogenic pressure. Moreover, the exceptionally preserved oxic-to-anoxic transitions in EM contribute to better understand older large-scale deoxygenation events (e.g., Paleozoic and Mesozoic Oceanic "Anoxic" Events).

1) It is shown that in restricted marine settings, climate and associated degree of surface-water freshening are the primary controls on deep-water dynamics, which in turn control the frequency and intensity of bottom-water deoxygenation, and the stability and depth of the chemocline. Warm and humid conditions (i.e., higher fresh-water inputs), as occurred during S5 and S7, promote more perennial restriction and stronger oxygen depletion in EM deep-waters than cooler and more arid conditions, as occurred during S6 and S8.
2) The deepest EM sites are the most vulnerable locations to develop deep-water restriction and deoxygenation. However, local hydrographic features (e.g., main active currents, proximity to continental borderlands, etc.) play an important role on the degree of deep-water restriction and deoxygenation. EM locations more influenced by ADW Outflow and EMDW currents develop weaker deep-water restriction and oxygen depletion than deep EM locations less influenced by these water-masses, which develop more stable deep-water restriction (i.e., less frequent deep-water renewal) and stronger deoxygenation.
3) Particulate shuttling was very intense in EM water-column during sapropel deposition, similar to the modern Cariaco Basin, which boosted burial fluxes of trace-metals influenced by this water-column process (e.g., Mo, Cu, Co, Ni, etc.).
4) Intensity in water-mass exchange between WM and EM plays a key role in EM deep-water oxygenation during sapropel deposition, controls Mo budget in EM water-masses (i.e., controls the intensity of the basin reservoir effect in EM) and is more intense during cold sapropel events.

Declaration of Competing Interest

The authors declare that they have no known competing financial interests or personal relationships that could have appeared to influence the work reported in this paper.

Data availability

Data will be made available on request.

Acknowledgment

This study is part of R. Monedero PhD project, and has been supported by Grants PID2019-104624RB-I00, PID2019-104625RB-100, and TED2021-131697B-C22 funded by MCIN/AEI/ 10.13039/501100011033, Grants FEDER/Junta de Andalucía P18-RT-3804 and P18-RT-4074, and by Research Groups RNM-179 and RNM-178 funded by Junta de Andaluca. We thank Prof. Adatte from Lausanne University (Switzerland) for Rock-eval analyses and TOC measurements. We are also grateful to the Center for Scientific Instrumentation (CIC, University of Granada) and the XRF Unit of the IACT (CSIC-UGR) for the ICP and XRF analyses, respectively. We are grateful to the Ocean Drilling Program for providing the analyzed samples as well as to the ODP Core Repository (Bremen, Germany) for assistance with sampling. We thank the Associate Editor, Dr. Mary Elliot, and the reviewer, Dr. Rick Hennekam, for their detailed and useful comments that significantly contributed to improve the manuscript.

Appendix A. Supplementary data

Supplementary data to this article can be found online at https://doi.org/10.1016/j.palaeo.2023.111601.

References

Abbott, O.J., 1977. The toxicity of ammonium molybdate to marine invertebrates. Mar. Pollut. Bull. 8, 204–205. https://doi.org/10.1016/0025-326X(77)90107-2.

Andersen, M.B., Matthews, A., Vance, D., Bar-Matthews, M., Archer, C., de Souza, G.F., 2018. A 10-fold decline in the deep Eastern Mediterranean thermohaline overturning circulation during the last interglacial period. EPSL. 503, 58–67. https://doi.org/10.1016/j.epsl.2018.09.013.

Andersen, M.B., Matthews, A., Bar-Matthews, M., Vance, D., 2020. Rapid onset of ocean anoxia shown by high U and low Mo isotope compositions of sapropel S1. Geochem. Perspect. Lett. 15, 10–14. https://doi.org/10.3929/ethz-b-000445569.

Algeo, T.J., Lyons, T.W., 2006. Mo-TOC covariation in modern anoxic marine environments: implication for analysis of paleoredox and paleohydrographic conditions. Paleoceanography 21, PA1016. https://doi.org/10.1029/2004PA001112.

Algeo, T.J., Lyons, T., Blakey, C., Over, J., 2007. Hydrographic conditions of the Devono-Carboniferous north American Seaway inferred from sedimentary Mo-TOC relationships. Palaeogeogr. Palaeoclimatol. Palaeoecol. 256, 204–230. https://doi.org/10.1016/j.palaeo.2007.02.035.

Algeo, T.J., Maynard, J.B., 2008. Trace metal covariation as a guide to water-mass conditions in ancient anoxic marine environments. Geosphere 4, 872–887. https://doi.org/10.1130/GES00174.1.

Algeo, T.J., Tribovillard, N., 2009. Environmental analysis of paleoceanographic systems based on molybdenum-uranium covariation. Chem. Geol. 268, 211–225. https://doi.org/10.1016/j.chemgeo.2009.09.001.

Algeo, T.J., Morford, J., Cruse, A., 2011. New applications of trace metals as proxies in Marine Paleoenvironments. Chem. Geol. 307, 160–164. https://doi.org/10.1016/j.chemgeo.2012.03.009.

Algeo, T.J., Rowe, H., 2012. Paleoceanographic applications of trace-metal concentration data. Chem. Geol. 324–325, 6–18. https://doi.org/10.1016/j.chemgeo.2011.09.002.

Algeo, T.J., Li, C., 2020. Redox classification and calibration of redox thresholds in sedimentary systems. Geochim. Cosmochim. Acta 287, 8–26. https://doi.org/10.1016/j.gca.2020.01.055.

Amitai, Y., Ashkenazy, Y., Gildor, H., 2018. The effect of wind-stress over the Eastern Mediterranean on deep-water formation in the Adriatic Sea. Deep Sea Res. Part II Top. Stud. Oceanogr. 164, 5–13. https://doi.org/10.1016/j.dsr2.2018.11.015.

Azrieli-Tal, I., Matthews, A., Bar-Matthews, M., Almogi-Labin, A., Vance, D., Archer, C., Teutsch, N., 2014. Evidence from molybdenum and iron isotopes and molybdenum–uranium covariation for sulphidic bottom waters during Eastern Mediterranean sapropel S1 formation. EPSL. 393, 231–242. https://doi.org/10.1016/j.epsl.2014.02.054.

Astraldi, M., Gasparini, G.P., 1992. The seasonal characteristics of the circulation in the North Mediterranean basin and their relationship with the atmospheric-climatic conditions. J. Geophys. Res. 97, 9531–9540. https://doi.org/10.1029/92JC00114.

Bea, F., 1996. Residence of REE, Y, Th and U in granites and crustal protoliths: implications for the chemistry of crustal melts. J. Petrol. 37, 521–532. https://doi.org/10.1093/petrology/37.3.521.

Behar, F., Beaumont, V., Penteado, H.L.De B., 2001. Rock-Eval 6 technology: performances and developments. Oil Gas Sci. Technol. 56, 111–134. https://doi.org/10.2516/ogst:2001013.

Benkovitz, A., Matthews, A., Teutsch, N., Poulton, S.W., Bar-Matthews, M., Almogi-Labin, A., 2020. Tracing water column euxinia in Eastern Mediterranean Sapropels S5 and S7. Chem. Geol. 545, 119627 https://doi.org/10.1016/j.chemgeo.2020.119627.

Berrang, P.G., Grill, E.V., 1974. The effect of manganese oxide scavenging on molybdenum in Saanich inlet, British Columbia. Mar. Chem. 2, 125–148. https://doi.org/10.1016/0304-4203(74)90033-4.

Bertine, K.K., Turekian, K.K., 1973. Molybdenum in marine sediments. Geochim. Cosmochim. Acta 37, 1415–1434. https://doi.org/10.1016/0016-7037(73)90080-X.

Blanchet, C., Tjallingii, R., Schleicher, A., Schouten, S., Frank, M., Brauer, A., 2020. Deoxygenation dynamics above the western Nile deep-sea fan during sapropel S1 at seasonal to millennial time-scales. Clim. Past 17, 1025–1050. https://doi.org/10.5194/cp-2020-114.

Böttcher, M., Effenberger, H., Gehlken, P.L., Grathoff, G., Schmidt, B., Geprägs, P., Bahlo, R., Dellwig, O., Leipe, T., Winde, V., Deutschmann, A., Stark, A., Gallego-Torres, D., Martinez-Ruiz, F., 2012. BaMn[CO3]2- a previously unrecognized double carbonate in low-temperature environments: Structural, spectroscopic, and textural tools for future identification. Chem. Erde 72, 85–89. https://doi.org/10.1016/j.chemer.2012.01.001.

Breitburg, D., Levin, L.A., Oschlies, A., Grégoire, M., Chavez, F.P., Conley, D.J., Garçon, V., Gilbert, D., Gutiérrez, D., Isensee, K., Jacinto, G.S., Limburg, K.E., Montes, I., Naqvi, S.W.A., Pitcher, G.C., Rabalais, N.N., Roman, M.R., Rose, K.A., Seibel, B.A., Telszewski, M., Yasuhara, M., Zhang, J., 2018. Declining oxygen in the global ocean and coastal waters. Science 359, 6371. https://doi.org/10.1126/science.aam7240.

Calvert, S.E., 1983. Geochemistry of Pleistocene sapropels and associated sediments from the Eastern Mediterranean. Oceanol. Acta 6, 255–267.

Calvert, S.E., Pedersen, T.F., 1996. Sedimentary geochemistry of manganese: implications for the environment of formation of manganiferous black shales. Econ. Geol. 91, 36–47. https://doi.org/10.2113/gsecongeo.91.1.36.

Calvert, S.E., Pedersen, T.F., 2007. Chapter fourteen elemental proxies for palaeoclimatic and palaeoceanographic variability in marine sediments: interpretation and application. Dev.Mar. Geo. 1, 567–644. https://doi.org/10.1016/S1572-5480(07)01019-6.

Camerlenghi, A., Ben, A., Huebscher, C., Forlin, E., Geletti, R., Brancatelli, G., Micallef, A., Saule, M., Facchin, L., 2019. Seismic markers of the Messinian salinity crisis in the deep Ionian Basin. Basin Res. 32 https://doi.org/10.1111/bre.12392.

Capotondi, L., Principato, M.S., Morigi, C., Sangiorgi, F., Maffioli, P., Giunta, S., Negri, A., Corselli, C., 2006. Foraminiferal variations and stratigraphic implications to the deposition of sapropel S5 in the eastern Mediterranean. Palaeogeogr. Palaeoclimatol. Palaeoecol. 235, 48–65. https://doi.org/10.1016/j.palaeo.2005.09.023.

Casford, J.S.L., Rohling, E.J., Abu-Zied, R.H., Jorissen, F.J., Leng, M., Thomson, J., 2003. A dynamic concept for eastern Mediterranean circulation and oxygenation during sapropel formation. Palaeogeogr. Palaeoclimatol. Palaeoecol. 190, 103–119. https://doi.org/10.1016/S0031-0182(02)00601-6.

Chiu, C.F., Sweere, T.C., Clarkson, M.O., de Souza, G.F., Hennekam, R., Vance, D., 2022. Co-variation systematics of uranium and molybdenum isotopes reveal pathways for descent into euxinia in Mediterranean sapropels. EPSL. 585, 117527 https://doi.org/10.1016/j.epsl.2022.117527.

Cita, M.B., Grignani, D., 1982. Nature and origin of Late Neogene Mediterranean sapropels. In: Academic, S.O., Schlanger, M.B. (Eds.), Nature and Origin of Cretaceous Carbon-Rich Facies, pp. 165–196. San Diego, California, USA.

Cita, M.B., Vergnaud-Grazzini, C., Robert, C., Chamley, H., Ciaranfi, N., Donofrio, S., 1977. Paleoclimatic record of a long deep-sea core from the eastern Mediterranean. Quat. Res. 8, 205–235. https://doi.org/10.1016/0033-5894(77)90046-1.

Crusius, J., Calvert, S., Pedersen, T., Sage, D., 1996. Rhenium and molybdenum enrichments in sediments as indicators of oxic, suboxic, and sulfidic conditions of deposition. Earth Planet. Sci. Lett. 145, 65–78. https://doi.org/10.1016/S0012-821X(96)00204-X.

De Lange, G.J., Middelburg, J.J., Pruysers, P.A., 1989. Discussion: Middle and Late Quaternary depositional sequences and cycles in the eastern Mediterranean. Sedimentology 36, 151–156.

Delanghe, D., Bard, E., Hamelin, B., 2002. New TIMS constraints on the uranium-238 and uranium-234 in seawaters from the main ocean basins and the Mediterranean Sea. Mar. Chem. 80, 79–93. https://doi.org/10.1016/S0304-4203(02)00100-7.

Dellwig, O., Leipe, T., März, C., Glockzin, M., Pollehne, F., Schnetger, B., Yakushev, E.V., Böttcher, M.E., Brumsack, H.J., 2010. A new particulate Mn-Fe-P-shuttle at the redoxcline of anoxic basins. Geochim. Cosmochim. Acta 74, 7100–7115. https://doi.org/10.1016/j.gca.2010.09.017.

Dermawan, D., Wang, Y.F., You, S.J., Jiang, J.J., Hsieh, Y.K., 2022. Impact of climatic and non-climatic stressors on ocean life and human health: a review. Sci. Total Environ. 821, 153387 https://doi.org/10.1016/j.scitotenv.2022.153387.

Emeis, K.C., Robertson, A.H.F., Richter, C., Shipboard Scientific Party, 1996. Proceedings of Ocean Drilling Programs (ODP). Initial. Rep. 160 https://doi.org/10.2973/odp.proc.ir.160.1996.

Emeis, K.C., Sakamoto, T., Wehausen, R., Brumsack, H.J., 2000. The sapropel record of the eastern Mediterranean Sea - results of Ocean Drilling Program Leg 160. Palaeogeogr. Palaeoclimatol. Palaeoecol. 158, 371–395. https://doi.org/10.1016/S0031-0182(00)00059-6.

Emeis, K.C., Schulz, H., Struck, U., Rossignol-Strick, M., Erlenkeuser, H., Howell, M.W., Kroon, D., Mackensen, A., Ishizuka, S., Oba, T., Sakamoto, T., Koizumi, I., 2003. Eastern Mediterranean surface water temperatures and delta O-18 composition during deposition of sapropels in the late Quaternary. Paleoceanography 18, 1–18. https://doi.org/10.1029/2000PA000617.

Fillippidi, A., De Lange, G.J., 2019. Eastern Mediterranean deep water formation during sapropel S1: a reconstruction using geochemical records along a bathymetric transect in the Adriatic outflow region. Paleoceanogr. and Paleoclimatol. 34, 409–429. https://doi.org/10.1029/2018PA003459.

Gallego-Torres, D., Romero, O., Martinez-Ruiz, F., Jung-Hyun, K., Donner, B., Ortega-Huertas, M., 2012. Evolution of deep-water redox conditions in the NW African upwelling system during the last glacial and deglaciation: implications for the deep ocean circulation. Quat. Res. 81, 330–338. https://doi.org/10.1016/j.yqres.2013.11.004.

Gallego-Torres, D., Martinez-Ruiz, de Lange, G., Jiménez-Espejo, F., Ortega-Huertas, M., 2007. Trace-elemental derived paleoceanographic and paleoclimatic conditions for Pleistocene Eastern Mediterranean sapropels. Palaeogeogr. Palaeoclimatol. Palaeoecol 293, 76–89. https://doi.org/10.1016/j.palaeo.2010.05.001.

Gallego-Torres, D., Martinez-Ruiz, F., Jiménez-Espejo, F., Ortega-Huertas, M., 2007. Pliocene-Holocene evolution of depositional conditions in the eastern Mediterranean: role of anoxia vs. productivity at time of sapropel deposition. Palaeogeogr. Palaeoclimatol. Palaeoecol. 246, 424–439. https://doi.org/10.1016/j.palaeo.2006.10.008.

Gallego-Torres, D., Martinez-Ruiz, F., Meyers, P., Jiménez-Espejo, F., Ortega-Huertas, M., 2010. Productivity patterns and N-fixation associated with Pliocene-Holocene sapropels: Paleoceanographic and paleoecological significance. Biogeosci. Discuss. 8, 415–431. https://doi.org/10.5194/bg-8-415-2011.

Giorgi, F., 2006. Climate change hot-spots. Geophys. Res. Lett. 33, L08707. https://doi.org/10.1029/2006GL025734.

Grant, K.M., Grimm, R., Mikolajewicz, U., Marino, G., Ziegler, M., Rohling, E.J., 2016. The timing of Mediterranean sapropel deposition relative to insolation, sea-level and African monsoon changes. Quat. Sci. Rev. 140, 125–141. https://doi.org/10.1016/j.quascirev.2016.03.026.

Grant, K.M., Rohling, E.J., Ramsey, C.B., Cheng, H., Edwards, R.L., Florindo, F., Heslop, D., Marra, F., Roberts, A.P., Tamisiea, M.E., Williams, F., 2014. Sea-level variability over five glacial cycles. Nat. Commun. 5, 5076. https://doi.org/10.1038/ncomms6076.

Grimm, R., Maier-Reimer, E., Mikolajewicz, U., Schmiedl, G., Muller-Navarra, K., Adloff, F., Grant, K.M., Ziegler, M., Lourens, L.J., Emeis, K.C., 2015. Late glacial

initiation of Holocene eastern Mediterranean sapropel formation. Nat. Commun. 6, 7099. https://doi.org/10.1038/ncomms8099.
Helz, G.R., Miller, C.V., Charnock, J.M., Mosselmans, J.F.W., Pattrick, R.A.D., Garner, C. D., Vaughan, D.J., 1996. Mechanism of molybdenum removal from the sea and its concentration in black shales: EXAFS evidence. Geochim. Cosmochim. Acta 60, 3631–3642. https://doi.org/10.1016/0016-7037(96)00195-0.
Hennekam, R., Jilbert, T., Schnetger, B., de Lange, G.J., 2014. Solar forcing of Nile discharge and sapropel S1 formation in the early to middle Holocene eastern Mediterranean. Paleoceanography 29, 343–356. https://doi.org/10.1002/2013PA002553.
Hennekam, R., van der Bolt, B., van Nes, E.H., de Lange, G.J., Scheffer, M., Reichart, G.J., 2020. Early-warning signals for marine anoxic events. Geophys. Res. Lett. 47 https://doi.org/10.1029/2020GL089183.
Higgs, N.C., Thomson, J., Wilson, T.R.S., Croudace, I.W., 1994. Modification and complete removal of eastern Mediterranean sapropels by postdepositional oxidation. Geology 22, 423–426. https://doi.org/10.1130/0091-7613(1994)022<0423:MACROE>2.3.CO;2.
Hilgen, F.J., 1991. Astronomical calibration of Gauss to Matuyama sapropels in the Mediterranean and implication for the geomagnetic polarity time scale. Earth Planet. Sci. Lett. 104, 226–244. https://doi.org/10.1016/0012-821X(91)90206-W.
Jacobs, L., Emerson, S., Skei, J., 1985. Partitioning and transport of metals across the O2/ H2S interface in a permanently anoxic basin: Framvaren Fjord, Norway. Geochim. Cosmochim. Acta 49, 1433–1444. https://doi.org/10.1016/0016-7037(85)90293-5.
Kidd, R.B., Cita, M.B., Ryan, W.B.F., 1978. Stratigraphy of eastern Mediterranean sapropel sequences recovered during Leg 42A and their paleoenvironmental significance. Initial Rep. Deep Sea Drill. Proj. 42A, 421–443. https://doi.org/10.2973/dsdp.proc.42-1.113-1.1978.
Lafargue, E., Marquis, F., Pillot, D., 1998. Rock-Eval 6 applications in hydrocarbon exploration, production, and soil contamination studies. Oil Gas Sci. Technol. 53, 421–437. https://doi.org/10.2516/ogst:1998036.
Lascaratos, A., Roether, W., Nittis, K., Klein, B., 1999. Recent changes in deep water formation and spreading in the eastern Mediterranean Sea: a review. Prog. Oceanogr. 44, 5–36. https://doi.org/10.1016/S0079-6611(99)00019-1.
Laskar, J., Joutel, F., Boudin, F., 1993. Orbital, precessional, and insolation quantities for the Earth from − 20 Myr to + 10 Myr. Astron. Astrophys. 270, 522–533.
Lathika, N., Rahaman, W., Tarique, M., Gandhi, N., Kumar, A., Thamban, M., 2021. Deep water circulation in the Arabian Sea during the last glacial cycle: implications for paleo-redox condition, carbon sink and atmospheric CO2 variability. Quat. Sci. Rev. 257 https://doi.org/10.1016/j.quascirev.2021.106853.
Levin, L.A., 2018. Manifestation, drivers, and emergence of open ocean deoxygenation. Annu. Rev. Mar. Sci. 10, 229–260. https://doi.org/10.1146/annurev-marine-121916-063359.
Lionello, P., Malanotte-Rizzoli, P., Boscolo, R., Alpert, P., Artale, V., Li, L., Luterbacher, J., May, W., Trigo, R., Tsimplis, M., Ulbrich, U., Xoplaki, E., 2006. The Mediterranean climate: an overview of the main characteristics and issues. Dev. Earth Environ. Sci. 4, 1–26. https://doi.org/10.1016/S1571-9197(06)80003-0.
Little, S.H., Vance, D., Lyons, T.W., McManus, J., 2015. Controls on trace metal authigenic enrichment in reducing sediments: insights from modern oxygen-deficient settings. Am. J. Sci. 315, 77–119. https://doi.org/10.2475/02.2015.01.
Liu, J., Algeo, T.J., 2020. Beyond redox: control of trace-metal enrichment in anoxic marine facies by watermass chemistry and sedimentation rate. Geochim. Cosmochim. Acta 287, 296–317. https://doi.org/10.1016/j.gca.2020.02.037.
Lourens, L.J., Antonarakou, A., Hilgen, F.J., Van Hoof, A.A.M., Vergnaud-Grazzini, C., Zachariasse, W.J., 1996. Evaluation of the Plio-Pleistocene astronomical time-scale. Paleoceanography 11, 391–413. https://doi.org/10.1029/96PA01125.
Malanotte-Rizzoli, P., Manca, B.B., d'Alcalà, M.R., Theocharis, A., Brenner, S., Budillon, G., Ozsoy, E., 1999. The eastern Mediterranean in the 80s and in the 90s: the big transition in the intermediate and deep circulations. Dyn. Atmos. Oceans 29, 365–395. https://doi.org/10.1016/S0377-0265(99)00011-1.
Marino, G., Rohling, E.J., Sangiorgi, F., Hayes, A., Casford, J.S.L., Lotter, A.F., Kucera, M., Brinkhuis, H., 2009. Early and middle Holocene in the Aegean Sea: interplay between high and low latitude climate variability. Quat. Sci. Rev. 28, 3246–3262. https://doi.org/10.1016/j.quascirev.2009.08.011.
Marino, G., Rohling, E.J., Rijpstra, W.I., Sangiorgi, F., Schouten, S., Sinninghe-Damsté, J. S., 2007. Aegean Sea as driver for hydrological and ecological changes in the eastern Mediterranean. Geology 35, 675–678. https://doi.org/10.1130/G23831A.1.
Matthews, A., Azrieli-Tal, I., Benkovitz, A., Bar-Matthews, M., Vance, D., Poulton, S.W., Teutsch, N., Almogi-Labin, A., Archer, C., 2017. Anoxic development of sapropel S1 in the Nile Fan inferred from redox sensitive proxies, Fe speciation, Fe and Mo isotopes. Chem. Geol. 475, 24–39. https://doi.org/10.1016/j.chemgeo.2017.10.028.
McArthur, J., 2019. Early Toarcian black shales: a response to an oceanic anoxic event or anoxia in marginal basins? Chem. Geol. 522, 71–83. https://doi.org/10.1016/j.chemgeo.2019.05.028.
McArthur, J., Algeo, T.J., van de Schootbrugge, B., Li, Q., Howarth, R.J., 2008. Basinal restriction, black shales, Re-Os dating, and the Early Toarcian (Jurassic) oceanic anoxic event. Paleoceanpgraphy 23, PA4217. https://doi.org/10.1029/2008PA001607.
Melki, T., Kallel, N., Fontugne, M., 2010. The nature of transitions from dry to wet condition during sapropel events in the Eastern Mediterranean Sea. Palaeogr. Palaeoclim. Palaeoecol. 291, 267–285. https://doi.org/10.1016/j.palaeo.2010.02.039.
Miller, A.R., 1963. Physical Oceanography of the Mediterranean Sea: a discourse. Rapp. Comm. Int. Mer Médit. 17, 857–887.
Millot, C., 1999. Circulation in the Western Mediterranean Sea. J. Mar. Syst. 20, 423–442. https://doi.org/10.1016/S0924-7963(98)00078-5.
Millot, C., 2009. Another description of the Mediterranean Sea outflow. Prog. Oceanogr. 82, 101–124. https://doi.org/10.1016/j.pocean.2009.04.016.
Millot, C., Taupier-Letage, I., 2005. Circulation in the Mediterranean Sea. In: Saliot, A. (Ed.), The Mediterranean Sea, pp. 26–66. https://doi.org/10.1007/b107143. Springer, Berlin, Heidelberg. Handb. Environ.Chem. 5.
Morford, J.L., Emerson, S., 1999. The geochemistry of redox sensitive trace metals in sediments. Geochim. Cosmochim. Acta 63, 1735–1750. https://doi.org/10.1016/S0016-7037(99)00126-X.
Morford, J.L., Emerson, S.R., Breckel, E.J., Kim, S.H., 2005. Diagenesis of oxyanions (V, U, Re, and Mo) in pore waters and sediments from a continental margin. Geochim. Cosmochim. Acta 69, 5021–5032. https://doi.org/10.1016/j.gca.2005.05.015.
Nijenhuis, I.A., Brumsack, de Lange, G.J., 1998. The trace element budget of the eastern mediterranean during pliocene sapropel formation. In: Proceedings of the Ocean Drilling Program, Scientific Results 160.. https://doi.org/10.2973/odp.proc.sr.160.019.1998.
Nolet, G.J., Corliss, B.H., 1990. Benthic foraminiferal evidence for reduced deep-water circulation during sapropel deposition in the eastern Mediterranean. Mar. Geol. 94, 109–130.
Ordoñez, L., Vogel, H., Sebag, D., Ariztegui, D., Adatte, T., Russell, J.M., Kallmeyer, J., Vuillemin, A., Friese, A., Crowe, S.A., Bauer, K.W., Simister, R., Henny, C., Nomosatryo, S., Bijaksana, S., 2019. Empowering conventional Rock-Eval pyrolysis for organic matter characterization of the siderite-rich sediments of Lake Towuti (Indonesia) using End-Member Analysis. Org. Geochem. 134 https://doi.org/10.1016/j.orggeochem.2019.05.002.
Osborne, A., Marino, G., Vance, D., Rohling, E.J., 2010. Eastern Mediterranean surface-water Nd during Eemian sapropel S5: monitoring northerly (mid latitude) versus southerly (sub tropical) freshwater contributions. Quat. Sci. Rev. 29, 2473–2483. https://doi.org/10.1016/j.quascirev.2010.05.015.
Ozsoy, E., 1981. On the atmospheric factors affecting the Levantine Sea. European Centre for Medium Range Weather Forecasts Reading, UK. Technical Report, 25, 29.
Passier, H.F., Middelburg, J.J., van Os, B.J.H., de Lange, G.J., 1996. Diagenetic pyritisation under eastern Mediterranean sapropels caused by downward sulphide diffusion. Geochim. Cosmochim. Acta 60, 751–776. https://doi.org/10.1016/0016-7037(95)00419-X.
Paul, K.M., van Heldmond, N.A.G.M., Slomp, C.P., Jokinen, S.A., Virtasalo, J.J., Filipsson, H.L., Jilbert, T., 2023. Sedimentary molybdenum and uranium: improving proxies for deoxygenation in coastal depositional environments. Chem. Geol. 615, 121203 https://doi.org/10.1016/j.chemgeo.2022.121203.
Pinardi, N., Masetti, E., 2000. Variability of the large scale general circulation of the Med- iterranean Sea from observations and modelling: a review. Palaeogeogr. Palaeoclimatol. Palaeoecol. 158, 153–173. https://doi.org/10.1016/S0031-0182(00)00048-1.
Pinardi, N., Zavatarelli, M., Adani, M., Coppini, G., Fratianni, C., Oddo, P., Simoncelli, S., Tonani, M., Lyubartsev, V., Dobricic, S., Bonaduce, A., 2015. Mediterranean Sea large-scale low-frequency ocean variability and water mass formation rates from 1987 to 2007: a retrospective analysis. Progress. Oceanogr. 132, 318–332. https://doi.org/10.1016/j.pocean.2013.11.003.
POEM group, 1992. General circulation of the eastern Mediterranean Sea. Earth Sci. Rev. 32, 285–308, 10.1016/0012-8252(92)90002-B.
Roether, W., Manca, B.B., Klien, B., Bregant, D., Georgopoulos, D., Beitzel, V., Kovacevic, V., Luchetta, A., 1996. Recent changes in Eastern Mediterranean deep waters. Science 271, 333–335. https://doi.org/10.1126/science.271.5247.333.
Rohling, E.J., 1994. Review and new aspects concerning the formation of Mediterranean sapropels. Mar. Geol. 122, 1–28. https://doi.org/10.1016/0025-3227(94)90202-X.
Rohling, E.J., Foster, G.L., Grant, K.M., Marino, G., Roberts, A.P., Tamisiea, M.E., Williams, F., 2014. Sea-level and deep-sea-temperature variability over the past 5.3 million years. Nature 508, 477–482. https://doi.org/10.1038/nature13230.
Rohling, E.J., Marino, G., Grant, K.M., 2015. Mediterranean climate and oceanography, and the periodic development of anoxic events (sapropels). Earth-Sci. Rev. 143, 62–97. https://doi.org/10.1016/j.earscirev.2015.01.008.
Rossignol-Strick, M., 1985. Mediterranean Quaternary sapropels, an immediate response of the African monsoon to variations of insolation. Palaeogeogr. Palaeoclimatol. Palaeoecol. 49, 237–263. https://doi.org/10.1016/0031-0182(85)90056-2.
Sainz de Murieta, E., Cunha, P., Cearreta, A., Murray, A., Buylaert, J.P., 2021. The Oyambre coastal terrace: a detailed sedimentary record of the Last Interglacial Stage in northern Iberia (Cantabrian coast, Spain). J. Quat. Sci. 36, 570–585. https://doi.org/10.1002/jqs.3317.
Scholz, F., 2018. Identifying oxygen minimum zone-type biogeochemical cycling in Earth history using inorganic geochemical proxies. Earth-Sci. Revs. 184, 29–45. https://doi.org/10.1016/j.earscirev.2018.08.002.
Scholz, F., Siebert, C., Dale, A.W., Frank, M., 2017. Intense molybdenum accumulation in sediments underneath a nitrogenous water column and implications for the reconstruction of paleo-redox conditions based on molybdenum isotopes. Geochim. Cosmochim. Acta 213, 400–417. https://doi.org/10.1016/j.gca.2017.06.048.
Schroeder, K., Chiggiato, J., Bryden, H., Borghini, M., Ismail, S.B., 2016. Abrupt climate shift in the Western Mediterranean Sea. Sci. Rep. 6, 23009. https://doi.org/10.1038/srep23009.
Sierro, F.J., Andersen, N., 2022. An exceptional record of millennial-scale climate variability in the southern Iberia margin during the MIS 6: impact on the formation of sapropel S6. Quat. Sci. Rev. 107527 https://doi.org/10.1016/j.quascirev.2022.107527.
Skliris, N., Lascaratos, A., 2004. Impacts of the Nile River damming on the thermohaline circulation and water mass characteristics of the Mediterranean Sea. J. Mar. Syst. 52, 121–143. https://doi.org/10.1016/j.jmarsys.2004.02.005.

Skliris, N., Marsh, R., Josey, S.A., Good, S.A., Liu, C., Allan, R.P., 2014. Salinity changes in the World Ocean since 1950 in relation to changing surface freshwater fluxes. Clim. Dyn. 43, 709–736. https://doi.org/10.1007/s00382-014-2131-7.

Sparnocchia, S., Manzella, G.M.R., Violette, P.E.L., 1994. The interannual and seasonal variability of the MAW and LIW core properties in the western Mediterranean Sea. Coast. Estuar. Stud. 46, 177–194. https://doi.org/10.1029/ce046p0177.

Sparnocchia, S., Schiano, E., Picco, P., Bozzano, R., Cappelletti, A., 2006. The anomalous warming of summer 2003 in the surface- layer of the Central Ligurian Sea (Western Mediterranean). Ann. Geophys. 24 https://doi.org/10.5194/angeo-24-443-2006.

Stocker, T.F., Qin, D., Plattner, G.K., Tignor, M., Allen, S.K., Boschung, J., Nauels, A., Xia, Y., Bex, V., Midgley, P.M., 2013. In: IPCC, 2013: Climate Change 2013: The Physical Science Basis. Contribution of Working Group I to the Fifth Assessment Report of the Intergovernmental Panel on Climate Change.. Cambridge Univ. Press, Cambridge, United Kingdom and New York, USA, p. 1535.

Sweere, S., van den Boorn, S., Dickson, A.J., Reichart, G.J., 2016. Definition of new trace-metal proxies for the controls on organic matter enrichment in marine sediments based on Mn Co, Mo and Cd concentrations. Chem. Geol. 441, 235–245. https://doi.org/10.1016/j.chemgeo.2016.08.028.

Sweere, T., Hennekam, R., Vance, D., Reichart, G.J., 2021. Molybdenum isotope constraints on the temporal development of sulfidic conditions during Mediterranean sapropel intervals. Geochem. Persp. Let. 17, 16–20. https://doi.org/10.7185/geochemlet.2108.

Tachikawa, K., Vidal, L., Cornuault, M., Garcia, M., Pothin, A., Sonzogni, C., Bard, E., Ménot, G., Revel, M., 2015. Eastern Mediterranean Sea circulation inferred from the conditions of S1 sapropel deposition. Clim. Past 11, 855–867. https://doi.org/10.5194/cp-11-855-2015.

Taylor, S.R., McLennan, S.M., 1995. The geochemical evolution of the continental crust. Rev. Geophys. 33, 241–265. https://doi.org/10.1029/95RG00262.

Tribovillard, N., Algeo, T.J., Baudin, F., Riboulleau, A., 2012. Analysis of marine environmental conditions based on molybdenum-uranium covariation applications to Mesozoic paleoceanography. Chem. Geol. 325, 46–58. https://doi.org/10.1016/j.chemgeo.2011.09.009.

Tribovillard, N., Algeo, T.J., Lyons, T., Riboulleau, A., 2006. Trace metals as paleoredox and paleoproductivity proxies: an update. Chem. Geol. 232, 12–32. https://doi.org/10.1016/j.chemgeo.2006.02.012.

Turco, M., Palazzi, E., Von Hardenberg, J., Provenzale, A., 2015. Observed climate change hotspots. Geophys. Res. Lett. 42, 3521–3528. https://doi.org/10.1002/2015GL063891.

van Santvoort, P.J.M., de Lange, G.J., 1996. Messinian salt fluxes into the present-day Eastern Mediterranean: implications for budget calculations and stagnation. Mar. Geol. 132, 241–251. https://doi.org/10.1016/0025-3227(95)00164-6.

van Santvoort, P.J.M., de Lange, G.J., Thomson, J., Cussen, H., Wilson, T.R.S., Krom, M. D., Strohle, K., 1996. Active post-depositional oxidation of the most recent sapropel (S1) in the eastern Mediterranean. Geochim. Cosmochim. Acta 60, 4007–4024. https://doi.org/10.1016/S0016-7037(96)00253-0.

Warning, B., Brumsack, H.J., 2000. Trace metal signatures of eastern Mediterranean sapropels. Paleogeogr. Paleoclimatol. Paleoecol. 158, 293–309. https://doi.org/10.1016/S0031-0182(00)00055-9.

Weldeab, S., Menke, V., Schmiedl, G., 2014. The pace of East African monsoon evolution during the Holocene. Geophys. Res. Lett. 41, 1724–1731. https://doi.org/10.1002/2014GL059361.

Wu, J., Böning, P., Pahnke, K., Tachikawa, K., de Lange, G., 2016. Unraveling North-African riverine and eolian contributions to Central Mediterranean sediments during Holocene sapropel S1 formation. Quat. Sci. Rev. 152, 31–48. https://doi.org/10.1016/j.quascirev.2016.09.029.

Wu, J., Fillipidi, A., Davies, G.R., de Lange, G., 2018. Riverine supply to the eastern Mediterranean during last interglacial sapropel S5 formation: a basin-wide perspective. Chem. Geol. 485, 74–89. https://doi.org/10.1016/j.chemgeo.2018.03.037.

Wüst, G., 1961. On the vertical circulation of the Mediterranean Sea. J. Geophys. Res. 66, 3261–3271. https://doi.org/10.1029/JZ066i010p03261.

Zheng, Y., Anderson, R.F., van Geen, A., Fleisher, M.Q., 2002. Preservation of particulate non-lithogenic uranium in marine sediments. Geochim. Cosmochim. Acta 66, 3085–3092. https://doi.org/10.1016/S0016-7037(01)00632-9.

Ziegler, M., Tuenter, E., Lourens, L.J., 2010. The precession phase of the boreal summer monsoon as viewed from the eastern Mediterranean (ODP Site 968). Quat. Sci. Rev. 29, 1481–1490. https://doi.org/10.1016/j.quascirev.2010.03.011.

Zirks, E., Krom, M.D., Zhu, D., Schmiedl, G., Goodman-Tchernov, B.N., 2019. In: ACS Earth Space Chem, 3, pp. 2287–2297. https://doi.org/10.1021/acsearthspacechem.9b00128.

Zwiep, K.L., Hennekam, R., Donders, T.H., Van Helmond, N.A., De Lange, G.J., Sangiorgi, F., 2018. Marine productivity, water column processes and seafloor anoxia in relation to Nile discharge during sapropels S1 and S3. Quat. Sci. Rev. 200, 178–190. https://doi.org/10.1016/j.quascirev.2018.08.026.